学位論文

Rydberg states of HgNe and HgAr as studied by optical–optical double resonance spectroscopy

光光二重共鳴分光法によるHgNeおよびHgArのリュードベリ状態の研究

1993年12月博士(理学)申請

東京大学大学院理学系研究科
相関理化学専攻

恩田　健

①

学位論文

Rydberg states of HgNe and HgAr as studied by optical–optical double resonance spectroscopy

光光二重共鳴分光法によるHgNeおよびHgArのリュードベリ状態の研究

1993年12月博士(理学)申請

東京大学大学院理学系研究科
相関理化学専攻

恩田 健

ACKNOWLEDGMENTS

The author would like to express his sincere gratitude to Professor Kaoru Yamanouchi for his continuous encouragement and valuable discussion, and supervising this thesis. The author also would like to express his sincere gratitude to Professor Soji Tsuchiya for his valuable discussion. The author indebted to Dr. Misaki Okunishi for valuable instruction in starting his research on HgRg vdW complex and his helpful advice. The author wishes to thank Professor Robert W. Field for his valuable discussion. The author wishes to thank Teruko Mabuchi for her collaboration of the research on $^1\Sigma^+$ Rydberg series.

CONTENTS

Chapter 1
General Introduction

I. Rydberg states of atoms and molecules

In a Rydberg state of atoms and molecules, a Rydberg electron is excited to a highly excited orbital whose mean radius is considerably large compared with a size of an ion core, which consists of the rest of electrons and an atomic nucleus (or atomic nuclei). Thus a dynamics of a Rydberg electron can be treated based on a simple picture in which one electron moves in an one–center Coulombic field generated by an ion core. A deviation from an ideal one–center Coulombic field is described by using a parameter δ, a quantum defect. For example, an energy level, E_{Ryd}, of a Rydberg state is represented as

$$E_{Ryd} = E_{Ip} - \frac{Ry}{n^{*2}} = E_{Ip} - \frac{Ry}{(n-\delta)^2} \quad , \qquad \text{(i)}$$

where Ry is the Rydberg constant and E_{Ip} is the ionization potential, and a mean radius of a Rydberg electron <r> can be scaled as $\langle r \rangle = \langle r \rangle_0 n^{*2}$. Even in the most advanced theory to treat a Rydberg state of atoms[1–3] and molecules[4–1], known as a multi–channel quantum defect theory (MQDT), a quantum defect is an important parameter to characterize a Rydberg state by quantitatively expressing non–adiabatic couplings among "channels" such as other Rydberg states, excited valence states and ionic states.

In most of the previous studies, experimental results have been successfully interpreted by MQDT, in other words, by determining quantum defects as practical parameters. However, as far as a molecular Rydberg state is concerned, only a limited number of studies have been reported so far, in which an essential dynamics of a Rydberg electron is extracted spectra. Such studies are all those on diatomic molecules and are categorized into the

following four cases;

(i) studies on H_2 by a non-empirical calculation[12-16],

(ii) studies on a large angular momentum (ℓ) state[17-23], such as d and f states of H_2 and NO, in which an interaction between a Rydberg electron and an ion core can be well-approximated only by a long range potential,

(iii) studies on CaF[24-26], in which an interaction between a Rydberg electron and an ion core can be well-approximated by an interaction between an Rydberg electron of Ca atom and a negative point charge,

(iv) studies on metal-rare gas van der Waals dimers (MRg)[27-39], such as HgNe.

In a Rydberg state of a MRg dimer, dynamics of a Rydberg electron can be investigated free from the effect of valence states because an energy difference between the first excited state of a rare gas ($\sim$17eV: Rg=Ne) and the ionization potential, Ip, of a metal atom ($\sim$10eV; M=Hg) is so large that valence orbitals are located far above Ip of a metal atom below which Rydberg states associated with a metal atom are located. The interaction between a Rydberg electron and an ion core in a diatomic molecule has been studied theoretically by a semiempirical pseudo-potential method[27-30] and an *ab initio* SCF method[31,32]. Experimentally an interatomic potential of Rydberg states for MgAr[33], CdAr[34,35], ZnAr[36], HgAr[37], HgNe[38], and AlAr[39,40] have been studied by laser spectroscopy. However, in these experimental studies, an investigation of an interaction between a Rydberg electron and an ion core was not a main concern and such an interaction was treated only qualitatively.

In the present thesis, the author chose HgNe and HgAr as the typical metal-rare gas dimers, and investigated their Rydberg states to extract an

essential dynamics of a Rydberg electron in a highly excited HgRg diatomic molecule by optical–optical double resonance (OODR) laser spectroscopy. One of the advantage of treating HgRg is that their Rydberg states can be studied in a wide energy region due to the nature of the lowest excited A and B states associated with $Hg(6^3P_1)$, which are used as intermediate states in the OODR scheme. From an analysis of the ro–vibronic structure of the OODR spectra, the author identifies and extracts two types of fundamental interactions between a Rydberg electron and an ion core which determine a characteristic feature of a dynamics of a Rydberg electron;

(i) an exchange interaction between a Rydberg electron and a rare gas atom characterizing an interatomic potential of an ion core,

(ii) an exchange and a spin–spin interaction between a Rydberg electron and an induced spin on a rare gas atom.

As described below, on the basis of the new experimental findings, the author proposes a consistent point of view to represent an interatomic potential of Rydberg states, and a mechanism of the spin induction on a rare gas atom.

II. Interatomic potential of Rydberg states of HgRg vdW dimers

II.1 Decomposition of the interatomic potential

In order to investigate the interaction between a Rydberg electron and an ion core, interatomic potentials having a different principal quantum number (n) and an orbital angular momentum quantum number (ℓ) are compared. Since the probability density distribution of a Rydberg electron depends on n and ℓ, the interaction between a Rydberg electron and an ion core can be varied by changing n and ℓ. In this thesis, interatomic potentials for the s–Rydberg series (n=7–10, ℓ=0), whose Rydberg electron distributes

spherically and penetrates deeply into the ion core, is investigated. From the systematic comparison of the determined interatomic potentials, a following model is proposed to describe the interatomic potential characteristic of a metal–rare gas molecule.

The interatomic potential (V_{Ryd}) is divided into two parts, i.e. the interatomic potential of an ion core (V_{ion}) and the repulsive potential (V_{ex}) originating from the exchange interaction between a Rydberg electron (n,ℓ) and a rare gas atom:

$$V_{Ryd}(n,\ell;R) = V_{ion}(R) + V_{ex}(n,\ell;R)\ , \qquad \text{(ii)}$$

where R represents an interatomic distance. Since the $V_{ion}(R)$ is independent of the Rydberg electron coordinates, the variation of the interatomic potential (V_{Ryd}) as a function of n and ℓ is ascribed to that of $V_{ex}(n, \ell; R)$. Assuming that the V_{ex} depends only on the electron density derived from the quantum defect orbital (QDO)[41,42], the shape of the determined potentials is consistently interpreted. A characteristic feature of this molecules is its straightforward prediction of the potential shape only from an ion core potential and a quantum defect of a metal atom. The experimental results are consistently interpreted based on this simple model for the interatomic potential.

II.2. S–Rydberg series of HgNe

The interatomic potentials of $^3\Sigma^+$ Hg(n^3S_1)Ne (n=7–10), which have a 6sns electronic configuration, are determined from the analysis of a vibrational structure of optical–optical double resonance (OODR) spectra.

As shown in Fig.1, the potential shape exhibits a characteristic dependence on the principal quantum number (n). At n=7, the potential has quasi-bound well and a hump above the dissociation limit. When n is changed from n=7 to n=8, the potential shape changes drastically, i.e. the quasi-bound well at n=7 changes to the relatively deep bound well at n=8. As n increases, the potential becomes deeper, but the shape of n=10 is very similar to that for n=9 and the potential for n=10 is only slightly deeper than that for n=9. This observation indicates that the potential almost converges to the ion core potential at n=10. On the basis of eq.(ii), the large hump observed at n=7 is ascribed to the strong exchange repulsion, $V_{ex}(r)$, at n=7. It is expected that V_{ex} becomes smaller as n increases and at n=10, V_{ex} is so small that the potential becomes almost identical to the ion core potential, $V_{ion}(r)$.

As shown in Fig.2, the n-dependence of a Rydberg electron density $|R(r)|^2$ (R(r): a radial wavefunction of Hg atom) calculated by QDO is almost parallel with the observed n-dependence of the interatomic potential. The density of the 7s electron is considerably large in a region from 2.5 to 7 Å, and then, a large exchange repulsion is expected in that region. When n increases by one, i.e. at n=8, the density decreases largely, but the amount of decrease from n=8 to n=9 is much smaller. At n=10, the density is so low that $V_{ex}(r)$ would be negligibly small. The good correlation between the observed potential shape and $|R(r)|^2$ indicates that an interatomic potential of MRg Rydberg state can be semi-quantitatively predicted by adding an ion core potential, $V_{ion}(r)$, and the exchange interaction $V_{ex}(r)$.

II.3. S-Rydberg series of HgAr

An interatomic potential of $^3\Sigma^+$ Hg(8^3S_1)Ar is determined and is

compared with that of $^3\Sigma^+$ Hg(8^3S_1)Ne. The potential of Hg(8^3S_1)Ar consists of one relatively deep well and its dissociation energy, D_e, is 1602 cm^{-1}, which is about 5 times as large as that of HgNe, 209 cm^{-1}. This difference of D_e between HgAr and HgNe is ascribed to that of ion core potentials, $V_{ion}(r)$. The attractive interaction to form $V_{ion}(r)$ originates mainly from the charge–charge induced interaction between Hg^+ and a rare gas atom. Since $HgAr^+$ has a stronger charge–charge interaction than $HgNe^+$, the interatomic potential of HgAr becomes deeper than that of HgNe.

The interatomic potential of Hg(7^3S_1)Ar^{39} has a shallow well, D_e=38 cm^{-1}, at longer interatomic distance, r_e=7Å, besides a deep well, D_e=1430 cm^{-1} located at r_e=2.9Å. Comparing the HgAr potential with the Rydberg electron density derived from QDO, the shallow well at n=7 can be interpreted as follows. The density of the 7s–Rydberg electron is confined in a region r < 6Å and the Rydberg electron shields the ion core from the Ar atom. Therefore, the outer shallow well is formed at around 7Å by an attractive dispersion interaction between the Rydberg Hg and Ar. The reason why the potential of HgNe has no shallow well is that the dispersion interaction in HgNe is not large enough to form such a shallow well.

III. The exchange and spin–spin interactions

III.1. Exchange interaction by the induced spin

The potentials of $^1\Sigma^+$ Hg(n^1S_0)Ne (n=7–9) are determined from the OODR spectra. The interatomic potentials both for the $^1\Sigma^+$ and the $^3\Sigma^+$ states having the same n are almost the same when $n \geqq 8$, and D_es' coincide with each other within 10 cm^{-1}. However, as shown in Fig.3, at n=7, the potentials for the singlet and the triplet states are different, i.e. the bottom of

the potential for $^3\Sigma^+$ lies 80 cm^{-1} above that for $^1\Sigma^+$. For an Hg atom, both $^3S_1$ and $^1S_0$ have the same electronic configuration, 6s7s, and the difference between these states should be caused by the exchange interaction between 6s and 7s. From the Pauli exclusion rule, when 6s and 7s electron spins are anti–parallel, these electrons can approach each other and when spins are parallel, they keep away from each other. Thus, the density of the 7s–electron of $Hg(^1S_0)$ near the ion core may be higher somewhat than that of $Hg(^3S_1)$. However, from the observed interatomic potentials, the electron density of $^1\Sigma^+$ in the region where the Ne atom is located is estimated to be lower than that of $^3\Sigma^+$ because V_{ex} has a positive correlation with the Rydberg electron density. These apparently contradicting situations is consistently interpreted by introducing an exchange interaction between a Rydberg electron and an induced spin on Ne. Even if the Rydberg electron density of $^3\Sigma^+$ is lower than that of $^1\Sigma^+$ by the Pauli exclusion rule, the exchange interaction between the induced spin on Ne and the Rydberg electron is strong enough to shift considerably upward the $^3\Sigma^+$ potential relative to the $^1\Sigma^+$ potential.

A mechanism of the spin induction on Ne is the kinetic exchange interaction[43,44]. This interaction is generated by a mixing between two electronic configurations, i.e. $(6s)^1(2p_z)^2$ and $(6s)^2(2p_z)^1$, where 6s and $2p_z$ are an orbitals of a Hg^+ ion and a Ne atom, respectively. The energy stabilization, ΔE, by inducing a spin through the kinetic exchange interaction is derived by a second–order perturbation from two electronic configurations:

$$\Delta E = -\frac{\left|\langle \Psi_1 | \mathbf{r}^{-1} | \Psi_2 \rangle\right|^2}{U} , \qquad \text{(iii)}$$

where Ψ_1 and Ψ_2 are wavefunctions of $(6s)^1(2p_Z)^2$ and $(6s)^2(2p_Z)^1$, respectively, and U is an energy difference between these two electronic configurations. Shown in Fig.4 is a schematic diagram of this mechanism. $HgNe^+$ can be compared with a MnO crystal having an antimagnetism by the kinetic exchange interaction;

$$Mn^{2+} + O^{2-} \rightarrow Mn^{+} + O^{-} \qquad U = +6 \text{ eV (in crystal)},$$
$$Hg^{+} + Ne \rightarrow Hg + Ne^{+} \qquad U = +12 \text{ eV (in gas phase)}.$$

Assuming the integral in eq.(iii) is the same for $HgNe^+$ and MnO, the stabilization energy for $HgNe^+$ would be approximately one half of MnO.

III.2. Spin–spin interaction by the induced spin

In order to derive more precise information on the induced spin on Ne, the rotational level structure of $^3\Sigma^+$ Hg(n^3S_1)Ne (n=7–9) is analyzed and a spin–spin constants, λ, are determined. The determined value of λ is 0.38 cm^{-1} for n=7, 0.28–0.15 cm^{-1} for n=8, and 0.00 for n=9. On the other hand, theoretically the value of λ derived from ss–electronic configuration should be zero. This difference can be interpreted by the spin–spin interaction between the induced spin on Ne and the Rydberg electron. The spin–spin constant of $^3\Sigma^+$ Hg(8^3S_1)Ne (v=0–3) decreases as a function of a vibrational quantum number, v. The values of λ are 0.28, 0.22, 0.20, and 0.15 cm^{-1} for v=0, 1, 2, and 3, respectively. This v–dependence of the spin–spin interaction is also explained by the kinetic exchange interaction. As the v increases, the interatomic distance increases because of a large unharmonicity, and as a consequence, an overlap between a 6s orbital of Hg^+ and a $2p_Z$

orbital of Ne decreases and so does the kinetic exchange interaction. This decrease of spin induction on Ne reduces the spin–spin interaction.

REFERENCES

1. M.J.Seaton, *Proc.Phys.Soc.*, **88**, 801 (1966).
2. M.J.Seaton, *Proc.Phys.Soc.*, **88**, 815 (1966).
3. M.J.Seaton, *Rep.Prog.Phys.*, **46**, 167 (1983).
4. U.Fano, *Phys.Rev.A*, **2**, 353 (1970).
5. C.Jungen and D.Dill, *J.Chem.Phys.*, **73**, 3338 (1980).
6. A.G–Suzor and C.Jungen, *J.Chem.Phys.*, **80**, 986 (1984).
7. C.H.Greene and Ch.Jungen, *Advances Atomic and Molecular Physics*, **21**, 51 (1985).
8. S.Sredin, D.Gauyacq, M.Horani, C.Jungen, G.Lefevre, and F.M–Seeuws, *Molecular Physics*, **4**, 825 (1987).
9. S.T.Pratt, J.L.Dehmer, and P.M.Dehmer, *J.Chem.Phys.*, 90, 2201 (1989).
10. S.T.Pratt, C.Jungen, and E.Miescher, *J.Chem.Phys.*, **90**, 5971 (1989).
11. E.F.McCormack, S.T.Pratt, P.M.Dehmer, and J.L.Dehmer, *J.Chem.Phys.*, **98**, 8370 (1993).
12. C.Jungen and O.Atabak, *J.Chem.Phys.*, **66**, 5584 (1977).
13. S.Kanfer and M.Shapiro, *J.Phys.B*, **16**, L655 (1983).
14. C.Mündel, M.Berman, and W.Domcke, *Phys.Rev.A*, **32**, 181 (1985).
15. G.Raseev, *J.Phys.B*, **18**, 423 (1985).
16. H.Gao, C.Jungen, and C.H.Greene, *Phys.Rev.A*, **47**, 4877 (1993).
17. C.Jungen and E.Miescher, *Can.J.Phys.*, **47**, 1769 (1969).
18. C.Jungen, *J.Chem.Phys.*, **53**, 4168 (1970).
19. R.S.Mulliken, *J.Am.Chem.Soc.*, **91**, 4615 (1969).
20. E.E.Eyler, Phys.Rev.A, 34, 2881 (1986).
21. C.Jungen, I.Dabrowski, G.Herzberg, and D.J.W.Kendall, *J.Chem.Phys.* **91**. 3926 (1989).
22. R Propin, *J.Phys.B*, 24, 4783 (1991).
23. P.W.Arcuni, *Phys.Rev.A*, 47, 4061 (1993).
24. S.F.Rice, H.Martin, and R.W.Field, *J.Chem.Phys.*, **82**, 5023 (1985).
25. J.E.Murphy,J.M.Berg,A.J.Merer,N.A.Harris, and R.W.Field, *Phys.Rev.Lett.*, **65**, 1861 (1990).
26.N.A.Harris and C.Jungen, *Phys.Rev.Lett.*, 70, 2549 (1993).
27. W.E.Baylis, *J.Chem.Phys.*, **51**, 2665 (1969).
28. J.Pascale and J.Vandeplanque, *J.Chem.Phys.*, 60, 2278 (1974).

29. M.E.Dolan and F.M–Seeuws, *J.Phys.B*, **14**, L583 (1981).
30. E. Czuchaj, H.Stoll and H.Preuss, *J.Phys.B*, 20, 1487 (1987).
31. M.Jungen and V.Staemmler, *J.Phys.B*, **21** 463 (1988).
32. J.A.Boatz, K.L.Bak, and J.Simons, *Theor.Chem.Acta.*, **83**, 209 (1993).
33. R.R.Bennett, J.G.McCaffrey, and W.H.Brechenridge, *J.Chem.Phys.*, **92**, 2740 (1990).
34. R.R.Bennett and W.H.Breckenridge, *J.Chem.Phys.*, **96**, 882 (1992).
35. M.Czajkowski, R.Bobkowski, and L.Krause, *Phys.Rev.A*, **45**, 6451 (1992).
36. R.R.Bennett and W.H.Breckenridge, *J.Chem.Phys.*, **92**, 1588 (1990).
37. M.–C.Duval, O.B.D'Azy, W.H.Breckenridge, C.Jouvet, and B.Soep, *J.Chem.Phys.*, **85**, 6324 (1986).
38. M.Okunishi, K.Yamanouchi, K.Onda, and S.Tsuchiya, *J.Chem.Phys.*, **98**, 2675 (1993).
39. Z.Fu, S.Massick,J.G.Kaup,O.B.D'Azy, and W.H.Breckenridge, *J.Chem.Phys.*, 97, 1683 (1992).
40. S.A.Heidecke, Z.Fu, J.R.Colt, and M.D.Morse, *J.Chem.Phys.*, **97**, 1692 (1992).
41. G.Simons, *J.Chem.Phys.*, **60**, 645 (1974).
42. I.Martin and G.Simons, *J.Chem.Phys.*, **62**, 4799 (1975).
43. P.W.Anderson, *Phy.Rev.*, 79, 350 (1950).
44. P.W.Anderson, *Solid State Physics*, **14**, 99 (1963).

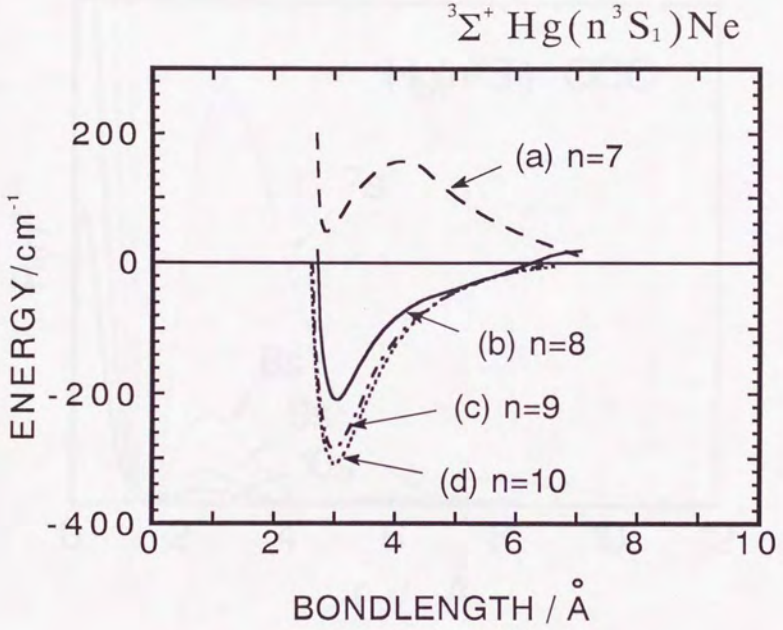

Fig.1 Interatomic potentials for $^3\Sigma^+$ Hg(n^3S_1)Ne (a) n=7, (b) n=8, (c) n=9, and (d) n=10.

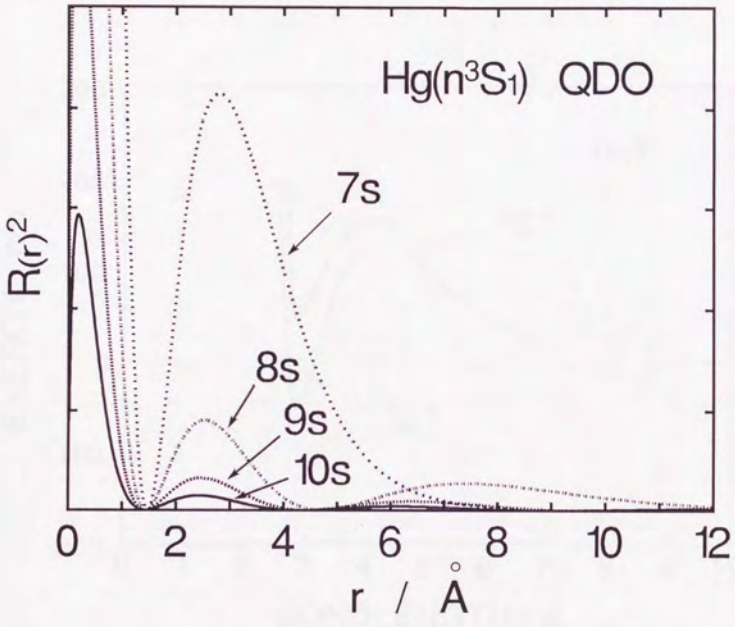

Fig.2 The density of a Rydberg electron of $Hg(n^3S_1)$ derived from QDO.

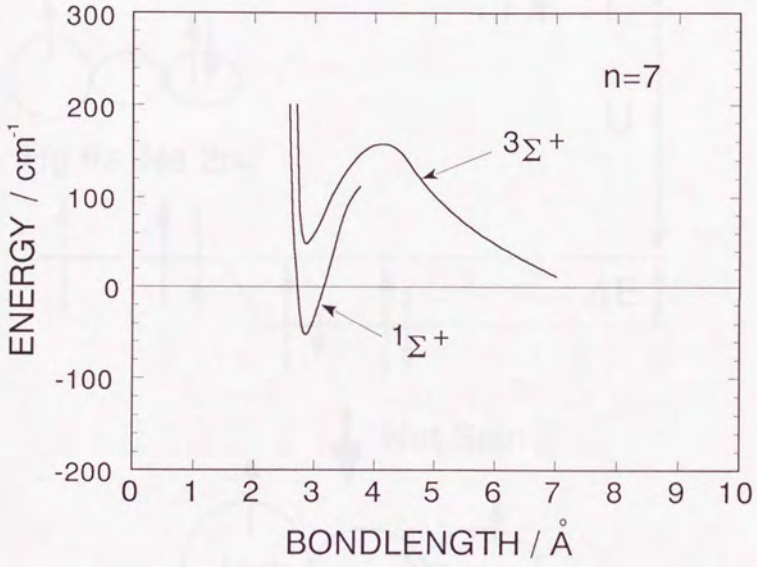

Fig.3 Interatomic potentials for $^3\Sigma^+$ Hg(7^3S_1)Ne and $^1\Sigma^+$ Hg(7^1S_0) Ne.

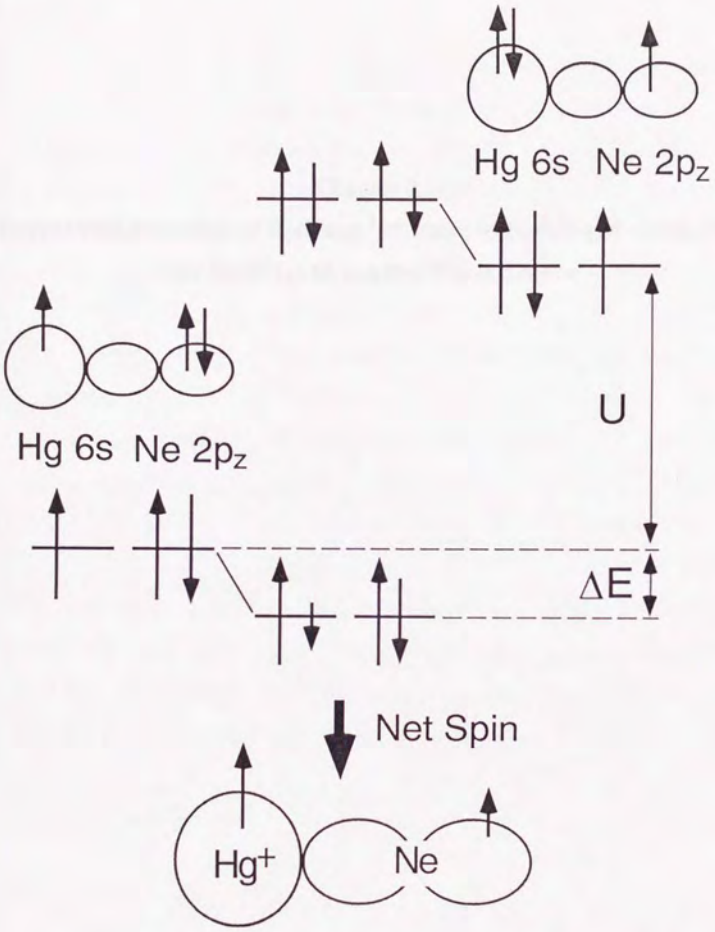

Fig.4 A schematic diagram for the spin induction on Ne by the kinetic exchange interaction.

Chapter 2

Interatomic potentials of Rydberg $^3\Sigma^+$ states of Hg(n^3S_1)Ne (n=8–10) and Hg(8^3S_1)Ar van der Waals dimers

ABSTRACT

The optical–optical double resonance (OODR) spectra of Rydberg $^3\Sigma^+$ states of Hg(n^3S_1)Ne (n=8–10) and Hg(8^3S_1)Ar are measured by using A and B states as intermediate states of the OODR process. The interatomic potentials of these states are determined over a wide range of the interatomic distance, 2–7Å, by the analysis of the vibrational structure. It is found that the potential shape varies sensitively with n and converges to that of the ion core, $HgNe^+$. Dissociation energies (D_e) for the n=8, 9 and 10 Rydberg states are 209(2) cm^{-1}, 284(2) cm^{-1} and 309(2) cm^{-1}, respectively. Using the quantum defect orbital (QDO) for a Hg atom, it is shown that the interatomic potential for the Rydberg states are expressed by the sum of the ion core potential, $V_{ion}(R)$, and the repulsive potential, $V_{ex}(R)$. It is found that $V_{ex}(R)$ originates mainly from the exchange repulsion between the Rydberg electron and the rare gas atom and has a close correlation with the density of a Rydberg electron, $|R(r)|^2$. A potential for Hg(8^3S_1)Ar, whose dissociation energy is 1602(4) cm^{-1}, is much deeper than that of Hg(8^3S_1)Ne correlated to the same Hg state. This rare gas dependence of the interatomic potential is also interpreted by expressing the potential as $V_{ion}(R) + V_{ex}(R)$.

I. INTRODUCTION

A metal–rare gas van der Waals (vdW) diatomic molecules, in which a metal atom (M) and a rare gas atom (Rg) is bound by a weak van der Waals force, is an ideal system to extract a characteristic dynamics of a Rydberg electron in a molecule. Since the lowest electronically excited state of a rare gas atom is usually located much higher in energy than an ionization potential of a metal atom, excited valence states of M–Rg are located above its ionization limit and are well–separated from the Rydberg states. Thus, by investigation of the Rydberg states of M–Rg, it is expected that dynamics of a Rydberg electron interacting with a diatomic ion core can be extracted free from a Rydberg–valence interaction.

Among the M–Rg vdW dimers, HgRg (Rg=He,Ne,Ar,Kr,Xe) molecules have been investigated intensively in this decade[1–11]. The lowest excited states, A and B, associated with Hg(6^3P_1) were investigated for HgHe[6,8,10], HgNe[5,8], HgAr[4,5,8], HgKr[5,11] and HgXe[6,7,11]. The C state[9] associated with Hg($^1P_1$) was investigated for HgNe, HgAr, HgKr and HgXe. The lowest Rydberg states of HgNe[1] and HgAr[2,3] associated with Hg(7^3S_1) were also studied by optical–optical double resonance (OODR) spectroscopy via the A and B states. Though both A and B states of HgRg correlate to the same excited state of Hg(6^3P_1), their interatomic potentials are very different from each other, i.e. the A state is more strongly bound than the B state and the equilibrium bond length, R_e, of the A state is much shorter than that of the B state. In the case of HgNe, the dissociation energy D_0 = 70 cm^{-1} and R_e = 3.49 Å for the A state, while D_0 = 11 cm^{-1} and R_e = 4.92 Å for the B state[8]. Therefore, by using these two states as intermediate states in the OODR scheme, a wide Franck–Condon region can be covered In other

words, an interatomic potential of higher lying Rydberg states can be investigated over a wide range of an interatomic distance.

Based on the OODR measurements, Duval et al.[3,4] reported that HgAr in the lowest Rydberg state, i.e. the $^3\Sigma^+$ state of Hg(7^3S_1)Ar, has a deep potential well (D_0 = 1430 cm^{-1}) as $HgAr^+$ (D_0=1630 cm^{-1})[2] and a shallow outer-well separated each other by a small hump with a barrier height of 15 cm^{-1} measured from the dissociation limit. Recently, Okunishi et al.[1] determined the characteristic interatomic potential of HgNe in the lowest Rydberg E $^3\Sigma^+$ state of Hg(7^3S_1)Ne by the OODR measurements; at an interatomic distance of 3.4 Å the interatomic potential has a relatively larger hump, whose height is 150 cm^{-1} measured from the dissociation limit. It was found that two quasi-bound states are trapped in the inner well and one resonantly trapped state is located around the energy near the top of the barrier. In these studies of HgAr and HgNe, the interatomic potentials of the lowest Rydberg states of HgAr and HgNe were interpreted by a superposition of a weak dispersion type interaction in the longer interatomic distance and a strong attractive ion-induced dipole interaction in the shorter interatomic distance, and it was noticed that the position of the hump is close to a mean radius of the 7s orbital of the Rydberg electron.

In the present study, in order to clarify a role of the Rydberg electron in determining the interatomic potential of the Rydberg states of M-Rg dimers, the OODR investigation is extended towards higher-lying $^3\Sigma^+$ Rydberg states, and the interatomic potentials of Hg(n^3S_1)Ne (n=8-10) and Hg(8^3S_1)Ar are determined precisely by the analysis of the OODR spectra. The observed dependence of an interatomic potential on a principal quantum number and a rare gas species attached to Hg is consistently interpreted by a

Rydberg electron density evaluated by using the quantum defect orbitals (QDO) of Hg(n^3S_1) (n=6–10).

II. EXPERIMENT

The experimental setup used in the present study is similar to that described in our previous report[1]. The HgNe and HgAr vdW dimers are produced respectively in a supersonic expansion of Ne and Ar carrier gas with a trace of Hg vapor through a heated fuel–injector type pulsed valve with a Hg reservoir. The stagnation pressure for Ne is ~7 atm and that for Ar is ~ 4atm. The nozzle temperature is kept at ~200℃ corresponding to the Hg vapor of 17 mTorr. The HgRg dimer is excited to their Rydberg states by the OODR process using the frequency–doubled output of two dye lasers (Lambda Phisik FL3002 and Molectron DL14P), which are simultaneously pumped by a XeCl excimer laser (Lambda Physik LPX 105i). The fluorescence emitted from the intermediate A and B states is monitored by a solar–blind photomultiplier (Hamamatsu R166UH), while the OODR fluorescence signal is detected by a photomultiplier (Hamamatsu R928) with a filter (Toshiba UV29) which efficiently cuts the fluorescence form the intermediate states. Since the wavenumbers of the vibrational transition from the ground state to the intermediate state were precisely determined using I_2 spectra by Yamanouchi et al.[8], the dye laser for this transition does not need to be calibrated. The dye laser for the transition from the intermediate state to the Rydberg state is calibrated by measuring simultaneously I_2 spectra and two HgNe transitions with high resolution (FWHM= ~ 0.08cm^{-1}). The transitions used for this purpose are Hg(8^3S_1)Ne (v=0) – A (v=0), 34436.01(5) cm^{-1}, and Hg(9^3S_1)Ne (v=1) – A (v=0), 38663.85(14) cm^{-1}.

III. RESULTS

III.1. Interatomic potentials of $^3\Sigma^+$ Hg(n^3S_1)Ne (n=8–10)

$^3\Sigma^+$ Hg(8^3S_1)Ne

Since the Rydberg state, Hg(8^3S_1)Ne, has a 6s8s electronic configuration, from which only $^3\Sigma^+$ and $^1\Sigma^+$ are derived, Hg(8^3S_1)Ne should be assigned to $^3\Sigma^+$. The intermediate states, A and B states, have a 6s6p electronic configuration. From this configuration, $^3\Pi^+$, $^3\Sigma^+$, $^1\Pi^+$, and $^1\Sigma^+$ are derived taking into account an exchange interaction and a projection of an orbital angular momentum. These states are split into 8 states by diagonal and non–diagonal matrix elements of a spin–orbit interaction; i.e. $^3\Pi_{0^-}$, $^3\Pi_{0^+}$, $^3\Pi_1$, $^3\Pi_2$, $^3\Sigma_1^+$, $^3\Sigma_{0^-}^+$, $^1\Pi_1$ and $^1\Sigma_0^+$, which are lined up according to energy from the lowest state, so these states are assinged to a, A, B, c, d, e, C, and D, respectively. In previous papers, Hund's case(c) notaion has been used for these states because of relatively strong spin–orbit interation, for example, $^30^+$, ^{31} stand for A and B state, respectively.

The OODR spectra of the Rydberg $^3\Sigma^+$ state of HgNe associated with Hg(8^3S_1) are measured via six intermediate vibrational states, i.e., v'=0,1,2 of the A^30^+ state and v'=0,1,2 of the B^31 state. In this paper, v' is used to label the vibrational quantum number for the intermediate A and B states, and v and v" are used for the vibrational labeling of the Rydberg state and the electronic ground state, respectively. Shown in Figs.1 (a)–(f) are the OODR spectra of the $^3\Sigma^+ \leftarrow$ A(v'=0,1,2) and $^3\Sigma^+ \leftarrow$ B(v'=0,1,2) transitions near the Hg($8^3S_1 \leftarrow 6^3P_1$) atomic transition. The spectra via the three vibrational levels of the A state consist of one simple progression whose spacing

decreases gradually from 45 to 13 cm^{-1} as energy increases. In Figs.1(b) and 1(c), two and three nodes are observed in the Franck–Condon (FC) intensity pattern. These nodes reflect those of the wavefunction of the intermediate v'=1 and 2 states of the A state.

As shown in Fig.1(d)–(f), each vibronic transition in the spectra via the three vibrational levels of B states splits into two peaks, a main peak and an additional small peak separated on the lower energy side of the main peak. The interval between the main peak and the associated additional peak gradually increases from 2.7(5) cm^{-1} to 3.4 (5) cm^{-1} as v increases from 4 to 9. If a perturbation from another state causes the split, the interval should vary irregularly. Thus, these two peaks do not represent perturbation but the rotational band contour. There is no other electronic state overlapping with this state, which also supports that a perturbation does not cause the split. In the spectra via both A and B state, the transitions to v=3–7 are observed. Since the wavenumber of these peaks in the spectra via A state are identical to those at top of main peaks in the spectra via B state, the top of the main peak is regarded as a band origin of the transitions via B state. Around the band origin, there are rotational transitions from low J' levels of B state, so the additional peak consists of those from high J' levels and there are few levels between the high J' levels and the low J' levels. There are two possibilities that the high J' levels and the low J' levels are prepared at B state simultaneously. (i) The rotational structure of B–X transition spreads over $\sim$3 cm^{-1} and consists of that for six Hg isotopes spilt by the volume effect [8]. While, the line width of the dye laser is $\sim$0.5 cm^{-1}. Thus, high J' rotational levels of an isotope and low J' levels of another isotope can be prepared. (ii) Since R–branch of the B–X transition has a head and turns back to the lower

energy side from there, the high J' levels of R–branch and the low J' levels of P,Q–branch can be prepared simultaneously by the laser fixing at a lower energy side from the head. In the spectra of $Hg(8^3S_1)Ar$, the split of a vibrational level is not observed shown in Fig.6, which supports that the split represents a band contour because HgAr has about a half rotational constant of HgNe and the interval of the split is expected to be smaller than that of HgNe.

The observed range of the interatomic distance (3–7Å), which is estimated by the intermediate state wavefunctions, should be wide enough to cover the v=0 wave function of the Rydberg states. Thus, the observation that the progression suddenly starts at the transition located at 73815 cm^{-1} in all the three spectra of the $^3\Sigma^+ \leftarrow A$ transition in Figs.1(a)–(c) means that the transition at 73815 cm^{-1} is assigned to that to the v=0 level of the $^3\Sigma^+$ state.

The interatomic potential of $^3\Sigma^+$ $Hg(8^3S_1)Ne$ is determined from the observed vibrational structures as described below. First, the spacings between the adjacent OODR transitions are plotted in the Birge–Sponer (BS) plot as shown in Fig.2(a). The spacing decreases linearly in the low vibrational quantum number region (v=0–4), but it begins to deviate gradually upward from the linear slope at around v=5. By a least–squares fit to the linear part (v=0–4) of the BS plot, the Morse potential parameter ω_e=54.1(5) cm^{-1} and $\omega_e x_e$=4.46(10) cm^{-1} are determined. The equilibrium interatomic distance, R_e=3.01(3) Å, is derived after a trial–and–error simulation of the FC patterns for the transitions to v=0–4. In the simulation, the Morse function having the determined ω_e and $\omega_e x_e$ are used for the $^3\Sigma^+$ state and the known Morse functions for the A and B states[8]. This R_e value is in good agreement with R_e=2.99(3)Å, which is converted from the rotational constants of the

v=0–3 levels determined by the rotational analysis of the OODR transitions[12]. Then, by assuming that the deviation from the Morse function is ascribed to the outer wall of the potential, the shape of the outer wall is determined by the RKR method[13]. The potential width, $R_+ - R_-$, for each vibrational state is calculated, where R_+ and R_- represent outer and inner classical turning points, respectively. Thus, the R_+ values are derived from the RKR width, $R_+ - R_-$, by assuming that R_- stays on the inner classical turning points of the Morse function. As shown in Table I, for v=0–4, the potential widths, $R_+ - R_-$, of the Morse function are consistent with those derived above by the RKR method. The determined potential function is drawn in Fig3(b), where the inner wall of the potential is that of the Morse function and the outer wall is a Spline fit to the R_+ values. The derived R_+ and R_- are listed in Table II.

The dissociation energy, D_0, of this state is calculated to be D_0=183(2) cm^{-1} by a simple relation,

$$D_0 = D_0'' + \nu(Hg) - \nu_{00}' \quad , \qquad (1)$$

where D_0'' = 37(2) cm^{-1} is the dissociation energy of the electronic ground state[8], ν_{00} = 73814.97(9) cm^{-1} is the v=0 level of the $^3\Sigma^+$ Rydberg state measured from that of the electronic ground state, and $\nu(Hg)$ = 73961.298 cm^{-1} is the term value of the 8^3S_1 level of Hg[15]. From D_0, the D_e =209(2)cm^{-1} is obtained by using the equation, $D_e = D_0 + \omega_e/2 - \omega_e x_e/4$ with the determined Morse parameters. The errors in D_0 and D_e mainly come from the error of D_0'' ($\pm$ 2cm^{-1}) in the electronic ground X state. The determined potential parameters are summarized in Table III.

$^3\Sigma^+$ Hg(9^3S_1)Ne

The four OODR spectra via the A(v'=0,1) and B(v'=0,1) states are measured. As shown in Figs.4(a)–(d), the OODR transitions to the v=0–11 levels of the $^3\Sigma^+$ state are identified from these four spectra. The observed FC patterns are similar to those of the corresponding spectra of Hg(8^3S_1)Ne. The interatomic potential is determined in a similar manner as for Hg(8^3S_1)Ne. The potential width, $R_+ - R_-$, are calculated for the v=0–11 levels by the RKR method. As shown in the BS plot in Fig.2(b), spacings are linear for v=0–5, and they begin to deviate upward smoothly from the linear slope at v=6. The Morse potential parameters ω_e = 54.8(5) cm^{-1} and $\omega_e x_e$ = 3.17(10) cm^{-1} are determined from this linear part of the BS plot. By the FC simulation for v=0–5, the equilibrium interatomic distance R_e = 3.00(3) Å is obtained. The potential shown in Fig.3(c) is drawn using an inner wall of the derived Morse potential and an outer wall determined from a Spline fit to the classical outer turning point, R_+, calculated from the RKR width assuming that R_- is on the inner wall. The derived R_+ and R_- are listed in Table IV. Using Eq.(1), D_e = 284(2) cm^{-1} is derived. The determined potential parameters are summarized in Table III.

$^3\Sigma^+$ Hg(10^3S_1)Ne

The observed OODR spectra via A(v'=0,1) and B(v'=0,1) are shown in Figs.5(a)–(d). By combining the progressions observed in these four spectra, the transitions to the v=0–12 vibrational levels are identified. The FC patterns of the observed progressions are similar to those in the corresponding OODR spectra of Hg(8^3S_1)Ne and Hg(9^3S_1)Ne. As shown in the BS plot in Fig.2(c), the spacings are linear for v=0–5 and they begin to deviate upward

smoothly from the linear slope at v=6. As is done for $Hg(8^3S_1)Ne$ and $Hg(9^3S_1)Ne$, the R_+-R_- values are derived for the v=0–12 levels by the RKR method. The Morse potential parameters ω_e=55.5(5) cm^{-1} and $\omega_e x_e$=2.85(5) cm^{-1} are determined from the linear part of the BS plot (v=0–5), and the R_e =3.00(3) Å is derived from the simulation of the FC–patterns. The potential is drawn by combining Morse inner wall and a Spline fit outer wall. The derived r_+ and r_- are listed in Table V. The D_e=309(2) cm^{-1} is determined by the Eq.(1). The potential parameters are summarized in Table II.

III.2 Interatomic potential of $^3\Sigma^+$ $Hg(8^3S_1)Ar$ state

The OODR spectra via the A(v'=4) and B(v'=3,5,7) states are measured. In all of these OODR spectra one simple vibrational progression are found and the nodes in the FC patterns reflect those of the vibrational wavefunction of the intermediate state. Shown in Figs.6 is an example of the OODR spectra via B(v'=7). Reflecting the deep $Hg(8^3S_1)Ar$ potential, a total of 39 vibrational levels are identified in the four OODR spectra. The interatomic potential for the $^3\Sigma^+$ state is determined by the similar procedure adopted for the $Hg(n^3S_1)Ne$ (n=8–10) potentials. The spacing decreases linearly for v=0–21, and it begins to deviate upward smoothly from the linear slope at around v=22. Since the transition peaks in the progression in the spectrum via A(v'=4) smoothly disappears as the transition energy decreases, the band origin transition to the v=0 level of the $^3\Sigma^+$ state can not be assigned simply to the lowest–energy member of the progression. So the vibrational quantum numbers are assigned as described below. First, assuming that the lowest energy peak observed at 72648 cm^{-1} in the spectra via A(v'=4) is v=0,

the Morse potential parameters ω_e and $\omega_e x_e$ are determined by a least-squares fit to the linear part of the BS plot. Then, the FC pattern of the OODR spectrum is calculated using the Morse functions for both $^3\Sigma^+$ and A state. By varying r_e for the Morse potential of the $^3\Sigma^+$ state as one variable parameter, the r_e value which describes best the observed FC pattern is determined. As a next step, the vibrational quantum number of the 72648 cm^{-1} peak is increased by one and the above procedure is repeated. After trying the assignment of up to v=4, it is found that the FC pattern is reproduced well only when the 72648 cm^{-1} peak is assigned to v=1. Based on this vibrational assignment, ω_e = 102(4) cm^{-1}, $\omega_e x_e$ = 1.77(40) cm^{-1}, and R_e = 2.83(3) Å are derived. The potential shown in Fig.7(b) is drawn using an inner wall of the determined Morse potential and an outer wall determined from a Spline fit to the classical outer turning point, R_+, calculated from the RKR width assuming that R_- is on the inner wall. The potential parameters determined from the above analysis are summarized in Table VI. The dissociation energy D_e=1602(4) cm^{-1} is determined by Eq.(1).

IV. DISCUSSION

IV.1 Interatomic potentials of Hg(n^3S_1)Ne (n=7-10)

In the previous the section, we observed a characteristic principal quantum number (n) dependence of the interatomic potentials of Hg(n^3S_1)Ne. In order to discuss this n-dependence, the potentials for Hg(n^3S_1)Ne (n=8-10) determined in the present study and the potential of Hg(7^3S_1)Ne determined by Okunishi et al.[1] are compared as shown in Fig.3. The

interatomic potential of Hg(7^3S_1)Ne lies above the dissociation limit and has a hump at around 3.9(1) Å. The dissociation energy, D_e, defined as $V(R = \infty) - V(R_e)$ is $-53cm^{-1}$, where $V(R = \infty)$ represents the potential energy at the dissociation limit, $V(R_e)$ does the potential energy at the bottom of the bound part of the potential, and R does the interatomic distance in this paper. When n is increased by one from n=7 to n=8, the potential shape changes drastically, i.e. the quasi-bound well at n=7 changes to the relatively deep bound well at n=8, whose dissociation energy, D_e, is 209 cm^{-1}. However, for n=8 a small hump is still expected at R=7-8 Å, because the potential curve lies above the dissociation limit for R>6 Å and becomes almost flat at around R≅7Å. At n=9, the potential becomes deeper (D_e=284 cm^{-1}) and no hump is identified. The shape of the potential for n=10 is almost identical to that for n=9, but dissociation energy for n=10 (D_e=309cm^{-1}) is slightly larger (by 25 cm^{-1}) than that for n=9. In Fig.8, D_e is plotted as a function of the effective principal quantum number, n*. The dissociation energy, D_e, increases largely from n=7 to n=8, but the slope becomes almost flat from n=9 to n=10, indicating that the dissociation energy converges to that of the $HgNe^+$ ion core, whose dissociation energy is estimated to be only slightly larger than D_e=309 cm^{-1} for n=10.

In order to interpret the characteristic n-dependence of the shape of the interatomic potential function for the Hg(n^3S_1)Ne Rydberg states, the interatomic potential of a Rydberg state, $V_{Ryd}(R)$, is divided into two parts as

$$V_{Ryd}(n, \ell; R) = V_{ion}(R) + V_{ex}(n, \ell; R) \quad , \qquad (2)$$

where V_{ion} is defined as $V_{Ryd}(R = \infty)$, corresponding with the interatomic

potential of an ion core, and $V_{ex}(R; n, \ell)$ is the residual part defined as $V_{Ryd}(R)-V_{ion}(R)$. In Eq.(2), n and ℓ (an orbital angular momentum quantum number) dependences of $V_{Ryd}(R)$ is all ascribed to $V_{ex}(n, \ell; R)$. Since D_e increases as n increases, $V_{ex}(n, \ell; R)$ should be positive in the observed range of the interatomic distance, 3–7Å. The positive component in the potential is expected to be originated from an exchange repulsion between the Rydberg electron and the rare gas atom attached to Hg.

For the interpretation of the interaction between the Hg Rydberg electron of Hg and Rg, a wavefunction of the Rydberg electron in Hg(n^3S_1) is evaluated first by using quantum defect orbital (QDO)[14,15] method, which Simons devised to represent a radial wavefunction for a Rydberg state, $\Psi(r)$. In this paper, r is used for an orbital radius of the Rydberg electron. A QDO contains only three parameters; n, ℓ and a quantum defect (δ), and is expressed as

$$r\Psi(r) = \left[\frac{Z\Gamma(n-\delta+\lambda+1)}{\Gamma(n-\delta+\lambda)}\right]^{1/2} \frac{\left[2Zr/(n-\delta)\right]^{\lambda+1}}{(n-\delta)\Gamma(2\lambda+2)} e^{-Zr/(n-\delta)}\, {}_1F_1\left[\lambda+1-n+\delta, 2\lambda+2, 2Zr/(n-\delta)\right], \quad (3)$$

where ${}_1F_1$ is a confluent hypergeometric function, Z is a charge of an ion core, and λ is defined by $\lambda = \ell - \mathrm{Int}(\delta)$, with Int($\delta$) being an integer nearest to δ. It is known that a nodal pattern in the small r region is not well described by the QDO, but for large r, the QDO is a good approximation of a SCF orbital[14].

An outer electronic configuration of the $^3S_1$ Rydberg series of Hg is 6sns. Since s–orbital is isotropic, there is no need to consider the angular part of the wavefunction. The density of Rydberg electron, $|\Psi(r)|^2$, of Hg evaluated by the QDO of Eq.(3) is plotted in Fig.9 for n=7–9. It is clearly shown that the Rydberg electron density strongly depends on the principal

quantum number (n) in a region of r < 7 Å. In the first order approximation, when $\Psi(r)$ is large, an interaction between Rydberg electron and rare gas is expected be large at an interatomic distance (R) around the radius of the Rydberg electron (r). In fact, the n–dependence of $|\Psi(r)|^2$ is similar to the n–dependence of $V_{Ryd}(R)$, i.e. $|\Psi(r)|^2$ decreases as n increases, and the decrease from n=7 to 8 is large. In order to show the correlation between the interatomic potential, $V_{Ryd}(R)$, and the Rydberg electron density, $|\Psi(r)|^2$, $V_{Ryd}(R=3.0Å)$ and $|\Psi(r=3.0Å)|^2$ are plotted in Fig.10. At R=3.0 Å, where the equilibrium interatomic distances of determined Rydberg potentials for all n are located. The straight line derived by a least–squares fit to all data points is also drawn in Fig.10. The positive linear–correlation between $|\Psi(r)|^2$ and V_{Ryd} indicates that V_{ex} is almost proportional to $|\Psi(r)|^2$. Thus, based on Eq.(2) the interatomic potential for the Rydberg state, V_{Ryd}, can be predicted from the ion core potential, V_{ion}, and the density of Rydberg electron derived by the QDO orbital, $|\Psi(r)|^2$.

The position of the hump of the interatomic potential also reflects the peak position of the Rydberg electron density, $|\Psi(r)|^2$. For n=7, the interatomic distance of the hump is 3.9 Å is similar to the peak position of $|\Psi(r)|^2$ located at 3.0Å. For n=8, the distance of the hump is 7–8 Å is almost identical to the peak position of $|\Psi(r)|^2$ at 7.6 Å. For n=9,10, no hump is observed because the peak position of $|\Psi(r)|^2$ is located outside of the region for the observed potential. The reason why the peak for n=7 slightly shifts to outside from the peak of the Rydberg electron density that the V_{ion} has a steep positive slope in the interatomic region, 3–5 Å.

IV.2 Interatomic potentials of Hg(n^3S_1)Ar (n=7,8)

As shown in Fig.7(b), the interatomic potential of $Hg(8^3S_1)Ar$ consists of only one deep well whose dissociation energy (D_e) is 1630(4) cm^{-1} and its equilibrium interatomic distance (R_e) is 2.83 Å. The potential for $Hg(8^3S_1)Ar$ is much deeper than that for $Hg(8^3S_1)Ne$, D_e=209 cm^{-1}, which shows that the interatomic potential strongly depends on a species of rare gas. The Eq.(2) is applied in order to interpret the rare gas dependence of the interatomic potential. We let the V_{ex} be independent of a rare gas species, although the exchange repulsion between a Rydberg electron and a rare gas is proportional to $\rho^{2/3}$, where ρ is the density of rare gas, if the rare gas can be regarded as free electron gas[16]. If so, the rare gas dependence of the interatomic potential is ascribed to the rare gas dependence of V_{ion}. The value of $V_{ex}(3.0)$=100cm^{-1} is derived by

$$V_{ex}(3.0) = V_{ion}(3.0) - V_{Ryd}(3.0) \ ,$$

using $V_{Ryd}(3.0) = -209\ cm^{-1}$ for $Hg(8^3S_1)Ne$, $V_{ion}(3.0) = -309\ cm^{-1}$ for $Hg(10^3S_1)Ne$, whose potential must be close to an unknown $HgNe^+$ potential because in Fig.10 the value of V_{Ryd} for n=10 is very close to that of $V_{Ryd}(3.0)$ at $|R(3.0)|^2=0$. And then, using the $V_{ex}(3.0)$ derived from HgNe and $V_{Ryd}(3.0) = -1500\ cm^{-1}$ for $Hg(8^3S_1)Ar$, $V_{ion}(3.0) = -1600\ cm^{-1}$ for HgAr is derived by

$$V_{ion} = V_{Ryd} + V_{ex} \ .$$

This value is very close to $V_{ion}(2.8) = 1630\pm100\ cm^{-1}$, which is D_e of $HgAr^+$ estimated using Morse function[17]. This result shows that the rare gas

dependence originates mainly from V_{ion}.

By another way, V_{ion} for $HgAr^+$ can be estimated from V_{ion} for $HgNe^+$. Based on electrostatic model, Hg^+ and Rg interact each other by a charge–charge induced dipole attractive interaction, whose energy, E_c, is expressed as

$$E_c = -C\alpha/R^4 \quad [19] , \qquad (4)$$

where α represents a polarizability. Assuming a repulsive wall is vertical like hard wall, $V_{ion}(R)$ is proportional to E_c. Using the polarizability for Ar and Ne are 1.63 $Å^3$, and 0.39 $Å^3$, respectively[20], and R = 3.0 Å, the dissociation energy $V_{ion}(3.0)$ is about $-1300\ cm^{-1}$ for $HgAr^+$ is derived by

$$V_{ion}(HgAr^+) = V_{ion}(HgNe^+) \times \frac{\alpha(Ar)}{\alpha(Ne)} . \qquad (5)$$

Although this method is crude, the value of V_{ion} is close to the $V_{ion} = -1600\ cm^{-1}$ derived from Eq.(2), which also indicates that the rare gas dependence originates mainly from V_{ion}.

The above model is applied for the interatomic potential for HgAr at n=7. As shown in Fig.7(a), the potential for $Hg(7^3S_1)Ar$ is shallower than that of $Hg(8^3S_1)Ar$. The dissociation energy (D_e) at n=7 is 1430 cm^{-1} [2], and that of n=8 is 1603 cm^{-1}. Based Eq.(2), since only V_{ex} depends on n, the difference of V_{ex} between n=7 and n=8, ΔV_{ex}, is derived by

$$\Delta V_{ex} = V_{Ryd}(n=7) - V_{Ryd}(n=8) .$$

For HgNe, ΔV_{ex} is 173 cm^{-1}, and for HgAr is ΔV_{ex} is 262 cm^{-1}. These two values are close, which shows the model is appropriate. The interatomic potential of $Hg(7^3S_1)Ar$ has a characteristic shape, i.e. there is one shallow well whose dissociation energy (D_e) is 38 cm^{-1} and equilibrium interatomic distance (R_e) is 6.95Å, and a hump whose height is 15 cm^{-1} is located at 4.5 Å2. On the other hand, the hump of $Hg(7^3S_1)Ne$ is located at 3.9Å. The deference of hump position between $Hg(7^3S_1)Ar$ and $Hg(7^3S_1)Ne$ is ascribed that the slope of V_{ion} of HgAr in this region is steeper than that of HgNe. When the positive slope of V_{ion} is steeper at a hump of V_{ex}, inside of a hump of V_{Ryd} (= V_{ion} + V_{ex}) becomes deeper than outside of that, so the top of hump moves to outside. The position of the shallow well is also explain by Eq.(2) and the Rydberg electron density $|\Psi(r)|^2$. As shown in Fig.9, the position is outside of the high density region 2–6 Å for n=7, so the interaction to produce the shallow well is a dispersion force.

V. CONCLUSION

(1) The OODR spectra of $^3\Sigma^+$ $Hg(n^3S_1)Ne$ (n=8–10) and $Hg(8^3S_1)Ar$ are observed. From the vibrational structures of these spectra, the interatomic potentials of these states are determined by combination of FC simulation using Morse function and RKR method. By using A and B states whose equilibrium interatomic distance is apart from each other as intermediate state for OODR process, the shape of potential is determined over a wide range of an interatomic distance. The dissociation energy of these potentials, D_e, is derived.

(2) It is found that a characteristic principal quantum number dependence (n) of the interatomic potential, i.e. the dissociation energy increases as n

increases and a slope of increase becomes flat from n=9 to n=10. In order to interpret this n–dependence, the interatomic potential of HgRg, $V_{Ryd}(R; n, \ell)$, is divided into two potentials: (i) the potential of ion core, $V_{ion}(R)$, which is independent of the distribution of Rydberg electron and (ii) the repulsive potential, $V_{ex}(R; n, \ell)$, which depends on the distribution of the Rydberg electron.

(3) By comparison of observed interatomic potentials and the quantum defect orbitals (QDO) of Hg Rydberg state, we clarify the correlation between the repulsive potential V_{ex} and the distribution of the Rydberg electron, i.e. V_{ex} is almost proportional to the density of electron of Hg, $|R(r)|^2$, which is evaluated by the QDO wavefunction. Based on this idea, it is shown that (i) the deference of interatomic potential between HgNe and HgAr originates mainly from the deference of V_{ion} (ii) the hump is produced by a balance between V_{ex} and V_{ion}, (iii) the origin of an outer shallow well of $Hg(7^3S_1)Ar$ is a dispersion force between excited Hg and Ar.

ACKNOWLEDGMENTS

The present study is supported in part by the Grant–in–Aid (No. 05453016) and that for the Priority Area (No.05237205) from the Japanese Ministry of Education.

REFERENCES

1. M.Okunishi, K.Yamanouchi, K.Onda, and S.Tsuchiya, *J.Chem.Phys.*, **95**, 2675 (1993).

2. M.Duval, O.B.D'Azy, W.H.Brechenridge, C.Jouvet, and B.Soep, *J.Chem.Phys.*, **85**, 6324 (1986).

3. W.H.Brechenridge, M.C.Duval, C.Jouvet, and B.Soep, *Chem.Phys.Lett.*, **122**, 181 (1985).

4. K.Fuke, T.Saito, and K.Kaya, *J.Chem.Phys.*, **79**, 2487 (1983).

5. K.Fuke, T.Saito, and K.Kaya, *J.Chem.Phys.*, **81**, 2591 (1984).

6. M.C.Duval, C.Jouvet, and B.Soep, *Chem.Phys.Lett.*, **119**, 317 (1985).

7. K.Yamanouchi, J.Fukuyama, H.Horiguchi, S.Tsuchiya, K.Fuke, T.Saito, and K.Kaya, *J.Chem.Phys.*, **85**, 1806 (1986).

8. K.Yamanouchi, S.Isogai, M.Okunishi, and S.Tsuchiya, *J.Chem.Phys.*, **88**, 205 (1988).

9. T.Tsuchizawa, K.Yamanouchi, and S.Tsuchiya, *J.Chem.Phys.*, **89**, 4646 (1988).

10. R.Van.Zee, S.C.Blankespoor, and T.S.Zwier, *Chem.Phys.Lett.*, **158**, 306 (1989).

11. M.Okunishi, H.Nakazawa, K.Yamanouchi, and S.Tsuchiya, *J.Chem.Phys.*, **93**, 7526 (1990).

12. K.Onda and K.Yamanouchi, to be published.

13. H.E.Fleming and K.N.Rao, *J.Mol.Spec.*, **44**, 189 (1972).

14. G.Simons, *J.Chem.Phys.*, **60**, 645 (1974).

15. I.Martin and G.Simons, *J.Chem.Phys.*, **62**, 4799 (1975).

16. W.E.Balyis, *J.Chem.Phys.*, **51**, 2665 (1969).

17. N.J.Bridge, *J.Mol.Spec.*, **42**, 370 (1972).

18. J.O.Hirchtelder, C.F.Curtiss and R.B.Bird, *Molecular Theory of Gases and Liquids*, John Wiley & Sons (1964).

19. A.Dalgarno and A.E.Kingston, *Proc.Roy.Soc. (London)*, **A259**, 424 (1961).

Table I. Potential widths ($R_+ - R_-$) for $^3\Sigma^+$ Hg(8^3S_1)Ne calculated by RKR and Morse.

v	$R_+ - R_-$ / Å	
	RKR	Morse
0	0.37	0.38
1	0.72	0.72
2	1.04	1.02
3	1.39	1.37
4	1.78	1.84
5	2.22	2.78
6	2.67	3.02
7	3.06	–
8	3.37	–
9	3.62	–
10	3.89	–
11	4.36	–

Table II. Values of classical turnig points R_+ and R_- and energy measured from the v=0 for $^3\Sigma^+$ Hg(8^3S_1)Ne potential.

v	R_-[a]	R_+[b]	energy / cm^{-1}
0	2.89	3.25	0
1	2.80	3.52	45
2	2.76	3.80	82
3	2.74	4.12	109
4	2.72	4.51	131
5	2.72	4.94	144
6	2.71	5.38	156
7	2.71	5.77	167
8	2.71	6.08	177
9	2.71	6.33	186
10	2.71	6.60	195
11	2.71	7.07	207

[a]inner wall of the Morse function.

[b]outer turnig point calculated from the RKR width, R_+-R_-, assuming that R_- is on inner wall of the Morse function.

Table III. Values of classical turnig points R_+ and R_- and energy measured from the v=0 for $^3\Sigma^+$ Hg(9^3S_1)Ne potential.

v	R_-[a]	R_+[b]	energy / cm^{-1}
0	2.81	3.21	0
1	2.76	3.45	48
2	2.71	3.65	91
3	2.68	3.88	127
4	2.66	4.12	156
5	2.65	4.40	180
6	2.64	4.70	200
7	2.63	5.04	226
8	2.63	5.42	232
9	2.63	5.84	242
10	2.63	6.27	252
11	2.63	6.67	259

[a]inner wall of the Morse function.

[b]outer turnig point calculated from the RKR width, R_+-R_-, assuming that R_- is on inner wall of the Morse function.

Table IV. Values of classical turnig points R_+ and R_- and energy measured from the v=0 for $^3\Sigma^+$ Hg(10^3S_1)Ne potential.

v	R_-[a]	R_+[b]	energy / cm^{-1}
0	2.89	3.25	0
1	2.80	3.52	50
2	2.76	3.80	94
3	2.74	4.12	133
4	2.72	4.51	165
5	2.72	4.94	193
6	2.71	5.38	217
7	2.71	5.77	235
8	2.71	6.08	250
9	2.71	6.33	263
10	2.71	6.60	272
11	2.71	7.07	279

[a]inner wall of the Morse function.

[b]outer turnig point calculated from the RKR width, R_+-R_-, assuming that R_- is on inner wall of the Morse function.

Table V. Potential parameters for the $^3\Sigma^+$ Hg(n^3S_1)Ne (n=7–10) and $^1\Sigma^+$ Hg(6^1S_0)Ne.

	ω_e / cm^{-1}	$\omega_e x_e$ / cm^{-1}	D_e / cm^{-1}	R_e/Å
$^1\Sigma^+$ Hg(6^1S_0)Ne[a]	10.5	1.6	46	3.90
$^3\Sigma^+$ Hg(7^3S_1)Ne[b]	–	–	–53	2.9(1)
$^3\Sigma^+$ Hg(8^3S_1)Ne	54.2(2)[c]	4.49(4)[c]	209(2)[d]	3.00(3)[e]
$^3\Sigma^+$ Hg(9^3S_1)Ne	55.1(4)[c]	3.20(6)[c]	284(2)[d]	3.00(3)[e]
$^3\Sigma^+$ Hg(10^3S_1)Ne	55.5(2)[c]	2.85(3)[c]	309(3)[d]	3.00(3)[e]

[a]reference 8.

[b]reference 1.

[c]the error is an uncertainty σ of the least square method.

[d]the error is estimated from Eq.(1).

[e]the error is estimated from trial–and–error FC simulation.

Table VI. Potential parameters for the $^3\Sigma^+$ Hg(n^3S_1)Ar (n=7,8).

	ω_e / cm^{-1}	$\omega_e x_e$ / cm^{-1}	D_e / cm^{-1}	R_e/Å
$^3\Sigma^+$ Hg(7^3S_1)Ar[a]	112(1)	2.01(1)	1430(7)	2.81(2)
$^3\Sigma^+$ Hg(8^3S_1)Ar	102(4)[b]	1.77(40)[b]	1602(4)[c]	2.83(3)[d]

[a]reference 2.

[b]the error is an uncertainty σ of the least square method.

[c]the error is estimated from Eq.(1).

[d]the error is estimated from trial-and-error FC simulation.

FIGURE CAPTIONS

Fig.1. Observed OODR spectra of $^3\Sigma^+$ Hg(8^3S_1)Ne. The intermediate states are (a) A(v=0), (b) A(v=1), (c) A(v=2), (d) B(v=0), (e) B(v=1) and (f) B(v=2). The wavenumber means the energy measured from the X (v=0) state.

Fig.2. BS plot for (a) $^3\Sigma^+$ Hg(8^3S_1)Ne, (b) $^3\Sigma^+$ Hg(9^3S_1)Ne, (c) $^3\Sigma^+$ Hg(10^3S_1)Nep. Straight line is drawn by the least square method using (a) v=0–4, (b) v=0–5, (c) v=0–5. The Morse parameters, ω_e, $\omega_e x_e$, are listed on Table I.

Fig.3. Potential curves for $^3\Sigma^+$ Hg(n^3S_1)Ne (n=7–10). The n=7 potential is drawn using parameters in the reference 1.

Fig.4. Observed OODR spectrum of $^3\Sigma^+$ Hg(9^3S_1)Ne via (a) A(v=0), (b) A(v=1), (c) B(v=0) and (d) B(v=1). The wavenumber means the energy measured from the X (v=0) state.

Fig.5. Observed OODR spectrum of $^3\Sigma^+$ Hg(10^3S_1)Ne via (a) A(v=0), (b) A(v=1), (c) B(v=0) and (d) B(v=1). The wavenumber means the energy measured from the X (v=0) state.

Fig.6. Observed OODR spectrum of $^3\Sigma^+$ Hg(8^3S_1)Ar via B(v=7). The wavenumber means the energy measured from the X (v=0) state.

Fig.7. Potential curves for (a) $^3\Sigma^+$ Hg(7^3S_1)Ar and (b) $^3\Sigma^+$ Hg(8^3S_1)Ar.

The potential for $^3\Sigma^+$ Hg(7^3S_1)Ar is drawn using parameters in the reference 2.

Fig.8. Dissociation energies (D_e) of $^3\Sigma^+$ Hg(n^3S_1)Ne (n=7–10) are plotted as a function of n^*. n^* is defined by $n-\delta$, where n is principal quantum number and δ is quantum defect.

Fig.9. The density of electron, $|\Psi(r)|^2$, of Hg(n^3S_1) (n=7–10) are plotted as a function of a radius of Rydberg electron. The wavefunction, $\Psi(r)$, is calculated based on Simons's quantum defect orbital[12,13].

Fig.10. The energy of the interatomic potential at 3.0 Å, $V_{Ryd}(3.0)$, is ploted as a function of a densitiy of electron at 3.0 Å, $|\Psi(r)|^2$.

Fig.1

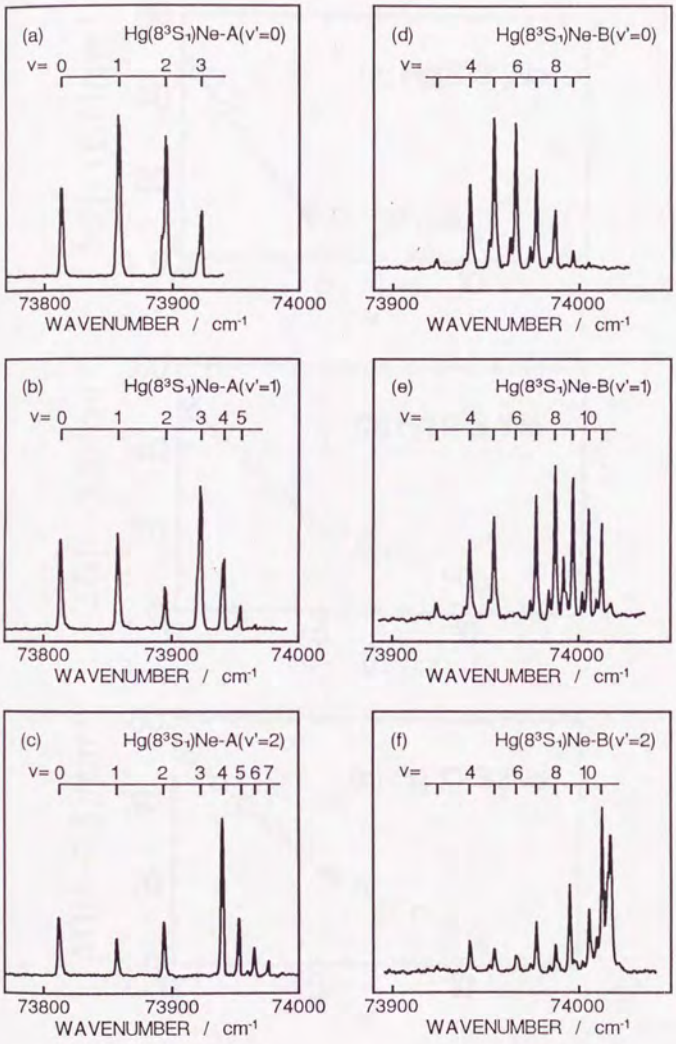
(a) Hg(8³S₁)Ne-A(v'=0)
v= 0 1 2 3
73800 73900 74000
WAVENUMBER / cm⁻¹
(d) Hg(8³S₁)Ne-B(v'=0)
v= 4 6 8
73900 74000
WAVENUMBER / cm⁻¹
(b) Hg(8³S₁)Ne-A(v'=1)
v= 0 1 2 3 4 5
73800 73900 74000
WAVENUMBER / cm⁻¹
(e) Hg(8³S₁)Ne-B(v'=1)
v= 4 6 8 10
73900 74000
WAVENUMBER / cm⁻¹
(c) Hg(8³S₁)Ne-A(v'=2)
v= 0 1 2 3 4 5 6 7
73800 73900 74000
WAVENUMBER / cm⁻¹
(f) Hg(8³S₁)Ne-B(v'=2)
v= 4 6 8 10
73900 74000
WAVENUMBER / cm⁻¹

Fig.2

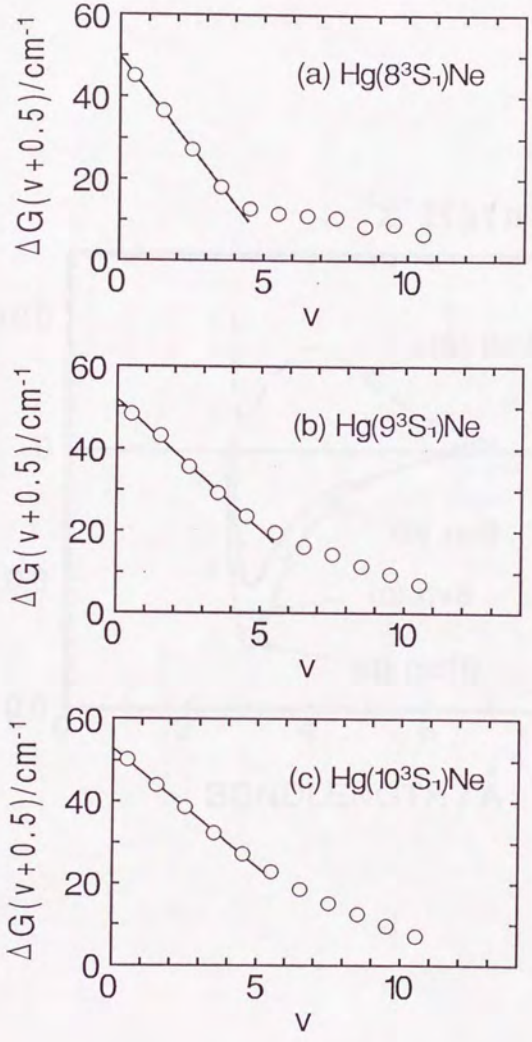

Fig.3

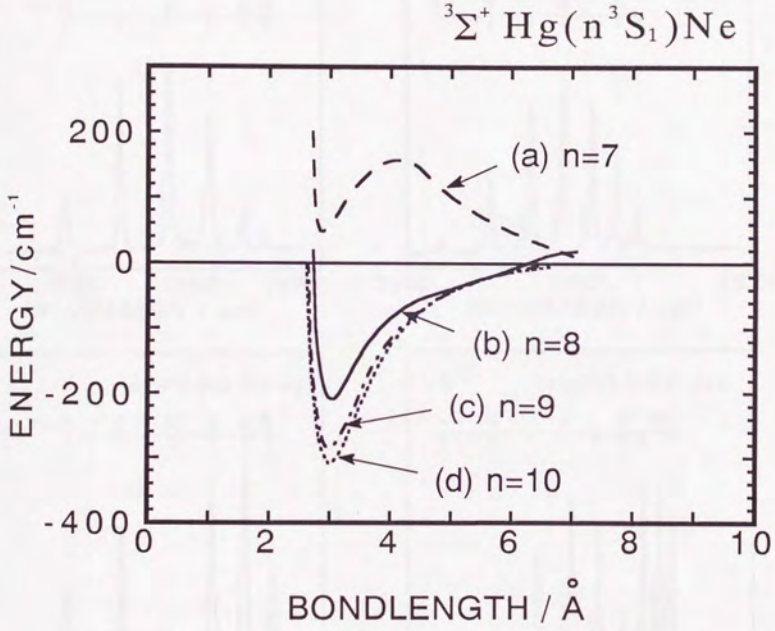
$^3\Sigma^+$ Hg(n^3S_1)Ne
200
0
-200
-400
ENERGY/cm^{-1}
(a) n=7
(b) n=8
(c) n=9
(d) n=10
0
2
4
6
8
10
BONDLENGTH / Å

Fig.4

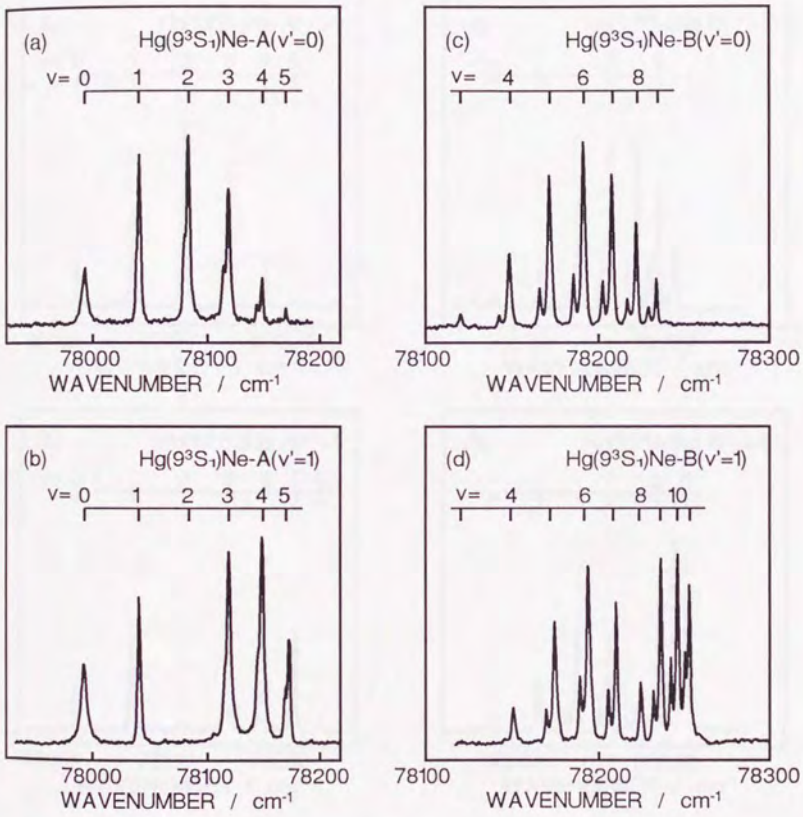
(a)
Hg(9³S₁)Ne-A(v'=0)
v= 0 1 2 3 4 5
78000 78100 78200
WAVENUMBER / cm⁻¹
(c)
Hg(9³S₁)Ne-B(v'=0)
v= 4 6 8
78100 78200 78300
WAVENUMBER / cm⁻¹
(b)
Hg(9³S₁)Ne-A(v'=1)
v= 0 1 2 3 4 5
78000 78100 78200
WAVENUMBER / cm⁻¹
(d)
Hg(9³S₁)Ne-B(v'=1)
v= 4 6 8 10
78100 78200 78300
WAVENUMBER / cm⁻¹

Fig.5

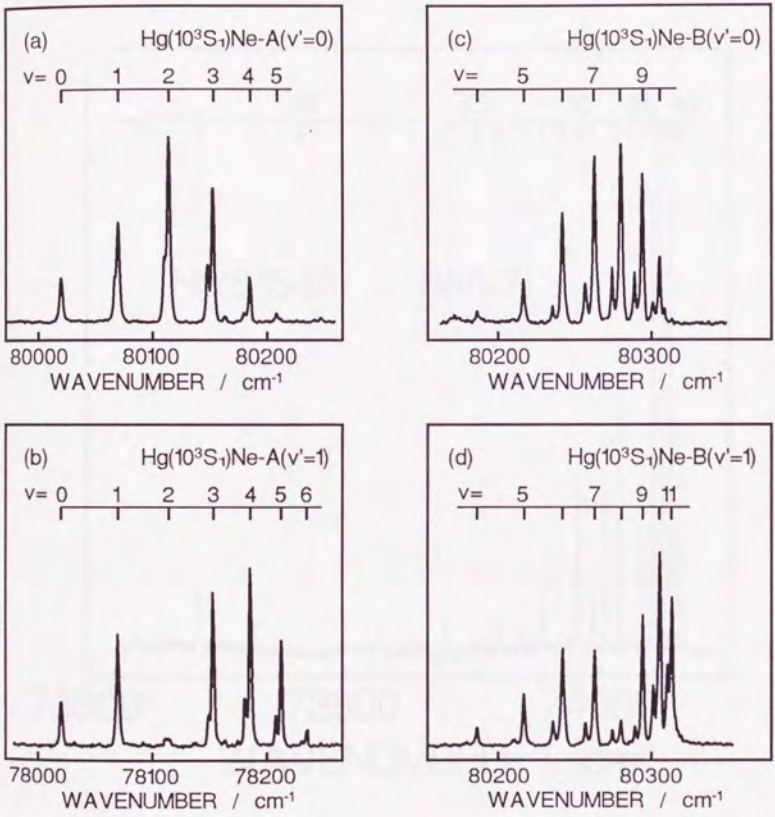
(a)
Hg(10³S₁)Ne-A(v'=0)
v= 0 1 2 3 4 5
80000 80100 80200
WAVENUMBER / cm⁻¹
(c)
Hg(10³S₁)Ne-B(v'=0)
v= 5 7 9
80200 80300
WAVENUMBER / cm⁻¹
(b)
Hg(10³S₁)Ne-A(v'=1)
v= 0 1 2 3 4 5 6
78000 78100 78200
WAVENUMBER / cm⁻¹
(d)
Hg(10³S₁)Ne-B(v'=1)
v= 5 7 9 11
80200 80300
WAVENUMBER / cm⁻¹

Fig.6

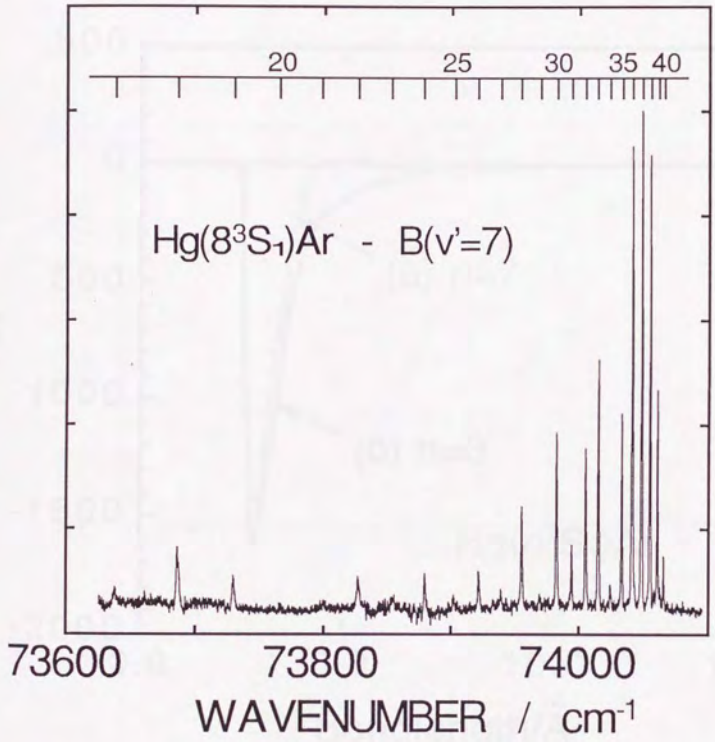

Fig.7

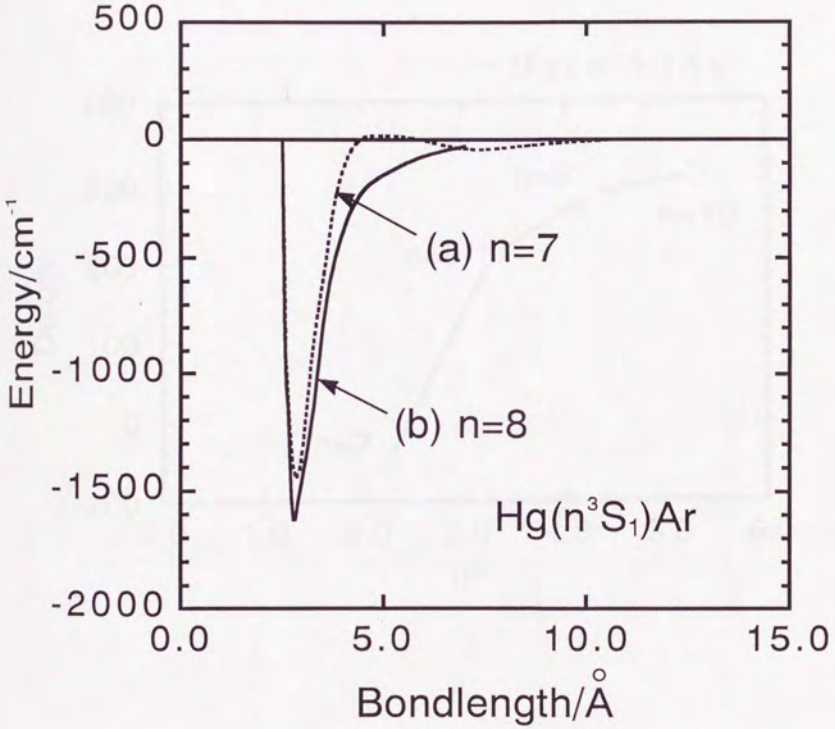
500
0
-500
-1000
-1500
-2000
Energy/cm-1
0.0
5.0
10.0
15.0
Bondlength/Å
(a) n=7
(b) n=8
Hg(n3S1)Ar

Fig.8

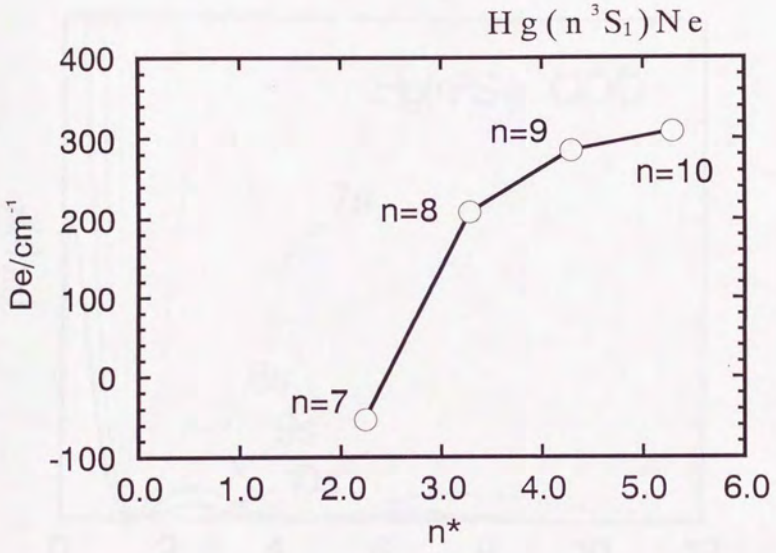
Hg(n³S₁)Ne
400
300
200
100
0
-100
De/cm⁻¹
0.0
1.0
2.0
3.0
4.0
5.0
6.0
n*
n=7
n=8
n=9
n=10

Fig.9

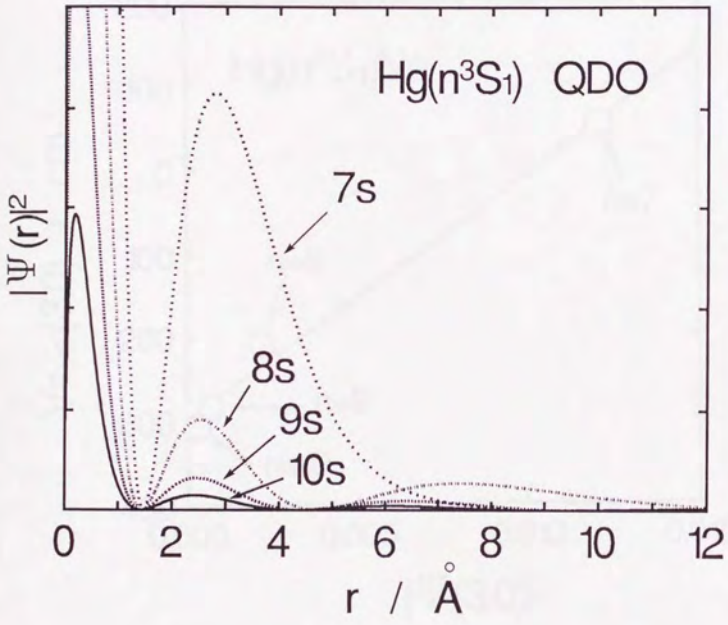

Fig.10

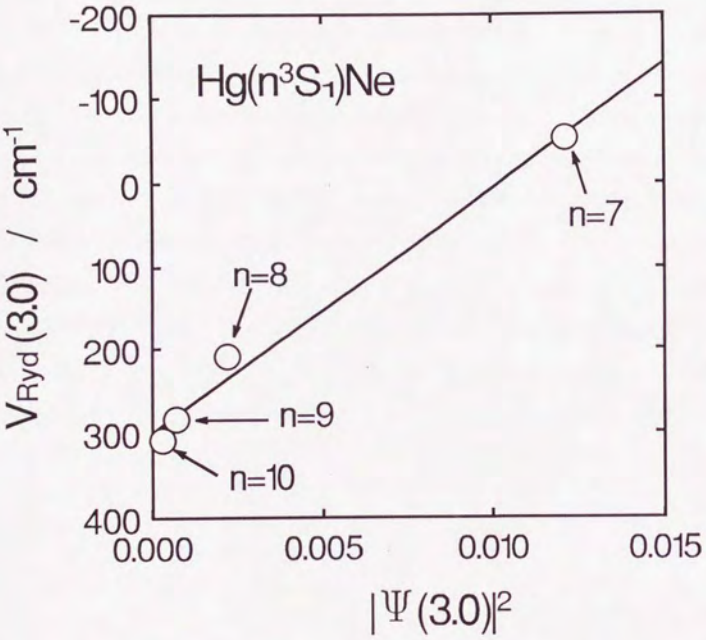
Hg(n³S₁)Ne
n=7
n=8
n=9
n=10
-200
-100
0
100
200
300
400
0.000
0.005
0.010
0.015
V_Ryd (3.0) / cm⁻¹
|Ψ(3.0)|²

Chapter 3

Spin-spin interaction of Rydberg $^3\Sigma^+$ states of Hg(n^3S_1)Ne (n=7-9) van der Waals dimer

ABSTRACT

High resolution optical–optical double resonance (OODR) spectra of $^3\Sigma^+$ states of Hg(n^3S_1)Ne (n=7–9) and Hg(8^3S_1)Ar are observed. The rotational structures are analyzed by a simulation taking into account the Hönl–London factor of $^3\Sigma^+$–$^3\Pi_{0^+}$ –$^1\Sigma^+$ transition and laser line width, and rotational constants (B_v) and spin–spin constants (λ) are determined. It is shown that the spin–spin constant depends on a principal quantum number (n): i.e. λ's for Hg(n^3S_1)Ne (n=7,8,9) are 0.38 cm^{-1}, 0.15 – 0.28 cm^{-1} and 0.00 cm^{-1}, respectively. This n–dependence is ascribed to increase of distance between Rydberg electron and ion core electron. The spin–spin constant also depends on the vibrational quantum number (n) in the Hg(8^3S_1)Ne state: i.e. 0.28, 0.22, 0.20 and 0.15 for v=0,1,2,3, respectively. Induced spin on the Ne by Hg^+ causes the v–dependence. The mechanism of the induction of spin on a closed shell rare gas by a metal ion can be explained by the kinetic exchange interaction. Line broadening by predissociation is observed in the Hg(9^3S_1)Ne and Hg(8^3S_1)Ar. The lifetimes estimated from the line width are < 20 ps for the Hg(9^3S_1)Ne and < 10 ps for Hg(8^3S_1)Ar.

I. INTRODUCTION

The mercury and rare gas diatomic van der Waals cluster (HgRg) is suitable for extracting the feature of Rydberg state. Since the first excited state of Rg (17eV: Rg=Ne) is much higher than the ionization potential, I.P., of Hg (10 eV), no valence state is located under the I.P. and there are only Rydberg states in highly excited states of HgRg. Thus, ro-vibronic states can be observed without perturbation of valence state. Besides there are well-studied A and B states[1] which are suitable for an intermediate state for optical-optical double resonance (OODR) spectroscopy.

By using these feature of HgRg vdW cluster, interatomic potential of Rydberg state for $^3\Sigma^+$ Hg(7^3S_1)Ne[2], $^3\Sigma^+$ Hg(n^3S_1)Ne(n=8-10)[3], and $^3\Sigma^+$ Hg(7^3S_1)Ar[4], $^3\Sigma^+$ Hg(8^3S_1)Ar[3] has been investigated. First, Duval et al.[4] reported that the lowest Rydberg state of HgAr, i.e. $^3\Sigma^+$ Hg(7^3S_1)Ar, has a deep potential well and a shallow outer-well separated each other by a small hump. They point out that a Rydberg electron is located around the position of hump so the deep well is close to $HgAr^+$ and a shallow well generates from the dispersion interaction. Recently, Okunishi et al. determined HgNe in the lowest Rydberg $^3\Sigma^+$ state of Hg(7^3S_1)Ne. The potential has a relatively large hump and two quasi-bound states inside the hump. This characteristic potential is interpreted by a balance of two interactions: i.e. attractive interaction of $HgNe^+$ ion core potential and repulsive exchange interaction between a Rydberg electron and a rare gas. Onda et al. determined the interatomic potentials in the $^3S_1$-Rydberg states of HgNe and HgAr in a wide energy region, i.e. $^3\Sigma^+$ Hg(n^3S_1)Ne (n=8-10) and $^3\Sigma^+$ Hg(8^3S_1)Ar. By a systematic study of the interatomic potentials, it is shown that a Rydberg

potential can be represented by sum of two potentials: i.e. the ion core potential and an repulsive potential generating from exchange repulsion between a Rydberg electron and a rare gas. Based on this point of view, principal quantum number (n) dependence of potential is ascribed to n-dependence of the exchange repulsion. The exchange repulsion can be predicted semi-quantitatively by a density of a Rydberg electron using the quantum defect orbital.

In the present study, in order to get more information on the Rydberg state of HgNe vdW dimer, we investigate systematically spin-spin interaction which is one of interaction between a Rydberg electron and an electron on the ion core. The spin-spin constant is determined by an analysis of the rotational structure in OODR spectra via A (v=0). Observed OODR spectra are $^3\Sigma^+$ Hg(7^3S_1)Ne (v=0,1), $^3\Sigma^+$ Hg(8^3S_1)Ne (v=0-3) and $^3\Sigma^+$ Hg(9^3S_1)Ne (v=1-3) having a different principal quantum number (n) and a vibrational quantum number (v) each other.

II. EXPERIMENT

The experimental setup for OODR is described in our previous paper[3]. The HgRg (Rg=Ne,Ar) van der Waal cluster are produced in a super sonic jet by using fuel injector with Hg reservoir heated 200℃. The carrier gas is Ne (or Ar) and the stagnation pressure is 4 atom. The HgRg is excited into Rydberg state by two dye lasers with intracavity étalon; Lambda Phisik FL3002 and Molectron DL14P. Both dye laser are pumped by an excimer laser (Lambda Physik LPX 105i), simultaneously. The fluorescence from intermediate state (~250 nm) is observed with a solar-blind photomultiplier (Hamamatsu R116). The fluorescence from Rydberg state is detected with

photomultiplier (Hamamatsu R928) with filter (Toshiba Y29) in order to cut the fluorescence from intermediate state. The resolution of both dye laser with etalon is 0.08 cm^{-1}. The frequency is calibrated by the iodine spectra recording simultaneously.

III. RESULTS

III.1. Analysis of rotational structures for $^3\Sigma^+$ Hg(8^3S_1)Ne (v=0,1,2,3)

In order to observe rotational resolved spectra of Rydberg state, the rotational structure of the intermediate has to be well investigated. Although the HgNe has small rotational constant and six isotope splitting by magnetic hyperfine and volume effect, the rotational structure is well studied by Yamanouchi et al.[4] As shown in Fig. 1, the rotational structure of A(v=0) – X(x=0) transition consists of six–isotope rotational structure, and the p–heads of 200, 202 and 204–isotope species are isolated. By using one of the isolated p–head, the rotational structure of Rydberg state can be observed as the single isotope rotational structure. However, the p–head of each isotopes is isolated in only A (v=0) – X (v=0) transition, so only vibrational states observed from A (v=0) state can be obtained as a single isotope rotational structure.

The OODR spectra of Hg(8^3S_1)Ne (v=0,1,2,3) states via the p–head of 202–isotope in A (v=0) state are observed as shown in Fig. 2 (a)–(d). Although the rotational structures of these state do not separate well, they look to consist of split P– and R–branch. Since the $^3\Sigma^+$ state is derived from 6s8s configuration of Hg(8^3S_1) and closed shell Ne, the origin of splitting comes form spin–spin interaction and spin–rotation interaction. We assign the unseparated rotational transition by simulation of the rotational structure.

In order to simulate these spectra, three factor have to be considered, i.e. rotational levels of $^3\Sigma^+$, Hönl–London factor of $^3\Sigma^+ - ^3\Pi_{0^+} - ^1\Sigma^+$ OODR process, and laser line width.

The rotational levels of a $^3\Sigma^+$ state were presented by Watson[5].

$$F_1 = B_v J(J+1) + (2\lambda + \gamma) + (B_v - \lambda - \tfrac{1}{2}\gamma) - [(B_v - \lambda - \tfrac{1}{2}\gamma)^2 + 4J(J+1)(B_V - \tfrac{1}{2}\gamma)^2]^{\frac{1}{2}} \quad \text{(III.1)}$$

$$F_2 = B_v J(J+1) + (2\lambda + \gamma) \quad \text{(III.2)}$$

$$F_3 = B_v J(J+1) + (2\lambda + \gamma) + (B_v - \lambda - \tfrac{1}{2}\gamma) + [(B_v - \lambda - \tfrac{1}{2}\gamma)^2 + 4J(J+1)(B_V - \tfrac{1}{2}\gamma)^2]^{\frac{1}{2}} \quad \text{(III.3)}$$

where B_v is a rotational constant, γ is a spin–rotation constant, and λ is a spin–spin constant. Since the spin–rotational interaction comes form the interaction between electron spin and rotation of core, it is small enough to neglect in the heavy molecule.

$^3\Sigma^+$ state is excited from ground state $^1\Sigma^+$ via A $^3\Pi_{0^+}$ in terms of case (a) representation, so the Hönl–London factor of OODR process is necessary for the simulation. We derived the Hönl–London factors of the $^3\Sigma^+$ (J) – $^3\Pi_{0^+}$ (J') – $^1\Sigma^+$ (J") in APPENDIX as follows:

$$I(^RQ,P)_{J''} \propto \mu_1^{\,2}\mu_2^{\,2}C_J^{\,2}(J''+1) \quad \text{(III.4)}$$

$$I(^RR,P)_{J''} \propto \mu_1^{\,2}\mu_2^{\,2}\frac{(J''+1)(4J''^2+1)}{(2J''+1)(2J''-1)} \quad \text{(III.5)}$$

$$I(^{P}P,P)_{J''} \propto \mu_1^2\mu_2^2 \frac{2(J''-2)(J''-1)(4J''^2+J''+12)}{(2J''+1)(2J''-1)^2} \qquad \text{(III.6)}$$

$$I(^{P}Q,P)_{J''} \propto \mu_1^2\mu_2^2 S_J^2(J''+1) \qquad \text{(III.7)}$$

where, for example, $I(^{R}Q,P)_{J''}$ is the Hönl–London factor for the successive excitation of a P–branch RQ–branch from a ground state having a rotational quantum number (J"), μ_1 and μ_2 are factors of first and second excitation respectively, which are common for all the rotational transitions.

Since p–head of A–X transition is excited by the second laser, the OODR intensities of each rotational line depend on the laser line width and the relative position between laser and rotational line. Therefore Lorentzian function as the second laser line shape (a solid line in the Fig. 1) multiplied by each rotational line.

The variable parameters are B_v, λ, rotational temperature (T_R), line width of rotational level, and the second laser line width and position. They are optimized by a trial–and–error method. The simulations of $Hg(n^3S_1)Ne$ (v=0,1,2,3) – A (v'=0) transitions and the assignment of each peak are shown in Fig. 2 (a)–(d). The calculated spectra are good agreement with observed spectra. Since the line width of rotational level, 0.08 cm^{-1}, is the same width as the dye laser determined by the Hg atomic transition, the broadening by predissociation is not observed.

In order to determine more precise rotational constants and spin–spin constants, we apply the non–linear least square fit of eq. (1) – (3) based on the above assignment. The variable parameters are band origin, Bv and l, and g fixes zero. The determined Bv, l and re calculated from Bv are listed in Table 1. The band origin is listed in Table 2.

III.2. Analysis of rotational structures for $^3\Sigma^+$ Hg(9^3S_1)Ne (v=1,2,3)

As shown in Fig. 3 (a) – (c), OODR spectra of Hg(9^3S_1)Ne (v=1,2,3) - A (v=0) are observed. Although all spectra in this state are broaden by predissociation, the rotational structure of v = 1 separates enough to reproduce the structure by simulation. Based on analysis of n=8, we optimize variable parameters; B_v, λ, T_R, line width of rotational level, and the second laser line width and position as shown in Fig. 3 (a). The band origin, Bv and l are determined by non–linear least square fit using the assignment of this simulation. The parameters are listed in Table 1, and the band origin is listed in Table 2. The predissociation lifetime is estimated from the FWHM of the rotational level is 20 ps. The line broadening strongly depends on vibrational quantum number. The rotational structure of v=2 and 3 are too broad to analyze but the rough estimated lifetime are 10ps and 5 ps respectively (Fig. 3 (b),(c)). The lifetimes are listed in Table 3.

III.3. Analysis of rotational structures for $^3\Sigma^+$ Hg(8^3S_1)Ne (v=0,1)

Although $^3\Sigma^+$ Hg(7^3S_1)Ne is quasi–bound state[2], the predisscoiation rate is so slow that the each rotational level is separated (Fig. 4 (a) and (b)). By using the equation of rotational level, eq. (1)–(3), and Hönl–London factor, eq. (4) – (7), the rotational structure is simulated as shown in Fig. 4 (a) and (b). The variable parameters, B_v, λ, T_R, line width of rotational level, and the second laser line width and position, are optimized by trial–and–error method. The band origin, B_v and λ determined by non–linear least square fit are listed Table 1 and 2. The assignment in the previous paper[2] is different from assignment determined by this method, but this assignment is correct.

III.4. Analysis of rotational structure for $^3\Sigma^+$ Hg(8^3S_1)Ar (v=2)

The rotational structure of $^3\Sigma^+$ Hg(8^3S_1)Ar – A (2,4) is observed. Although the $^3\Sigma^+$ Hg(8^3S_1)Ne is stable, the predissociation of HgAr is too fast to resolve rotational structure as shown in Fig. 5. The lifetime of the predissociation is less than 10ps by rough estimation based on the simulation.

IV. DISCUSSION

IV.1. Principal Quantum Number Dependence of Spin–Spin Interaction

Before a spin–spin interaction of HgNe is discussed, a relation between the determined spin–spin constant and a spin–spin interaction has to be shown. In general, a spin–spin constant determined from an experiment, λ_{exp}, originates both from a spin–spin interaction and from a second–order spin–orbit interaction [6], so the λ_{exp} can be written by

$$\lambda_{exp} = \lambda_{ss} + \lambda_{so}, \qquad \text{(IV.1)}$$

where λ_{ss} is a constant for a spin–spin interaction and λ_{so} is a constant for a second–order spin–orbit interaction. However, the spin–spin constant of $^3\Sigma^+$ Hg(n^3S_1)Ne represents only a pure spin–spin interaction because there is no spin–orbit matrix element between $^3\Sigma^+$ and $^1\Sigma^+$ states derived from an electronic configuration, 6sns.

In order to clarify a feature of a spin–spin interaction of a HgNe Rydberg state, a principal quantum number (n) dependence is investigated. The spin–spin constant for v=1 of each electronic state is chosen to study the n–dependence because λ depends on a vibrational quantum number. The

constant is plotted in Fig.6 as a function of the mean radius of Rydberg electron estimated from scaling rule[10]. At the lowest Rydberg state, n=7, the spin–spin interaction, λ=0.38(6) cm^{-1} is largest. When n changes from 7 to 8, λ decreases to 0.22(5) cm^{-1}. The interaction becomes almost zero at n=9. Assuming that the spin–spin interaction of $^3\Sigma^+$ Hg($^3S_1$)Ne is an interaction between an ion core electron (6s) and a Rydberg electron (ns), the n-dependence is ascribed to the distance between 6s and ns, i.e. as the n increases, the distance between increase and the interaction decrease.

In order to discuss more quantitatively, the spin–spin constants of these state are calculated from a Rydberg wavefunction of Hg atom. The λ is represented by using $|^3\Sigma^+_{+1}\rangle$, as following equation[7],

$$\langle {}^3\Sigma^+_{+1}|\mu|{}^3\Sigma^+_{+1}\rangle = \frac{2}{3}\lambda\left[3S_z^2 - S(S+1)\right]$$

$$= \frac{2}{3}\lambda \qquad \text{(IV.2)}$$

The Hamiltonian H^{SS} is written as[8]

$$H^{ss} = -\beta^2 \frac{3z_{12}^{\ 2} - r_{12}^{\ 2}}{r_{12}^{\ 5}}\left[2s_{1z}s_{2z} - \frac{1}{2}\left(s_1^{\ +}s_2^{\ -} + s_1^{\ -}s_2^{\ +}\right)\right] \qquad \text{(IV.3)}$$

Assuming the perturbation of Ne is small enough to neglect, the wavefunction of $^3\Sigma^+$ can be represented by using 6s and ns orbital of Hg atom and Slater determinant.

$$|^3\Sigma^+> = |\phi_{6s}\alpha\ \phi_{ns}\alpha| \qquad \text{(IV.4)}$$

where ϕ_{6S} and ϕ_{nS} are the wavefunction of Hg 6s and ns orbital, respectively. The matrix element eq. (IV.2) can be determined from the Hamiltonian, (IV.3), and the wavefunction, (IV.4), as follows[8].

$$<{}^3\Sigma^+ \mid H^{SS} \mid {}^3\Sigma^+> = \frac{2}{5}\beta^2 \int_0^\infty \phi_{6s}{}^2(r_1)dr_1 \int_{r_1}^\infty \frac{1}{r_2^3}\phi_{ns}{}^2(r_2)dr_2 \qquad \text{(IV.5)}$$

We use following quantum defect orbital derived by Simons[9] as the wavefunctions of Hg, ϕ_{6S} and ϕ_{nS},

$$\phi_{n\sigma}(r) = \left[\frac{Z\Gamma(n-\delta+\lambda+1)}{\Gamma(n-\delta+\lambda)}\right]^{1/2} \frac{\left[2Zr/(n-\delta)\right]^{\lambda+1}}{(n-\delta)\Gamma(2\lambda+2)} e^{-Zr/(n-\delta)}\, {}_1F_1\left[\lambda+1-n+\delta, 2\lambda+2, 2Zr/(n-\delta)\right] \qquad \text{(IV.6)}$$

By numeric integration, the λ's of ${}^3\Sigma^+$ Hg(n^3S_1)Ne (n=7–9) are calculated. The observed and calculated λ are listed Table 4.

The calculated spin–spin constants are 0.023 cm^{-1} for n=7, 0.0051 cm^{-1} for n=8 and 0.0018 cm^{-1} for n=9. The calculated λ decreases as n increases in the similar manner as the observed λ. The spin–spin interaction depends on overlap 6s and ns orbital, thus a spin–spin interaction decreases as n increases. Although the tendency to decrease is similar to the calculated value, the absolute value is more than ten times as large as the calculated value. This observed large spin–spin interaction can be explained by assuming the induced spin on Ne by Hg^+ ion. The Ne atom is close to a Rydberg electron enough to generate large spin–spin interaction, for example, 3.98 Å is mean radius of 7s orbital and 2.9 Å is equilibrium interatomic distance between Hg^+ and Ne.

A spin is induced on Ne by Hg^+ by the kinetic exchange interaction[11]. This interaction generates from a mixing between two electronic configurations, i.e. $(6s)^1(2p_Z)^2$ and $(6s)^2(2p_Z)^1$, where 6s is a orbital of Hg^+ ion and $2p_Z$ is a orbital of Ne atom. The energy to stabilize the induced spin, ΔE, by the kinetic exchange interaction is derived by a second-order perturbation from two electronic configurations:

$$\Delta E = -\frac{\left|\langle \Psi_1 | \mathbf{r}^{-1} | \Psi_2 \rangle\right|^2}{U} \qquad \text{(IV.7)}$$

where Ψ_1 and Ψ_2 are wavefunctions of $(6s)^1(2p_Z)^2$ and $(6s)^2(2p_Z)^1$, respectively, and U is a energy difference between two electronic configurations. $HgNe^+$ is compared with MnO crystal having anti-ferromagnetism by the kinetic exchange interaction.

$$Mn^{2+} + O^{2-} \rightarrow Mn^+ + O^- \qquad +6 \text{ eV in crystal}$$
$$Hg^+ + Ne \rightarrow Hg + Ne^+ \qquad +12 \text{ eV in gas phase}$$

Assuming the integrals in Eq.(IV.7) are the same, since the energy of $HgNe^+$ is twice as large as that of MnO, the $HgNe^+$ has approximately a half energy of the kinetic interaction of MnO.

IV.2. Vibrational Quantum Number Dependence of Spin-Spin Interaction

The spin-spin interaction of $^3\Sigma^+$ $Hg(8^3S_1)Ne$ strongly depends on the vibrational quantum number as shown in Fig.7. The λ for v=0 is 0.28 cm^{-1} and as v increases, λ decreases 10-25 %. In general, the v-dependence of λ

is ascribed to the v-dependence of an electronic configuration[7]. For example, a spin-spin constant of B $^3\Sigma^+$ state of O_2[12] strongly depends on v, i.e. when v changes from v=15 to v=16, λ increase 25 %. If λ of $^3\Sigma^+$ Hg(8^3S_1)Ne originates from a single configuration, 6s8s, this v-dependence cannot be explained. Thus, a configuration mixing should be considered.

By comparing between observed and calculated λ in the preceding section, it is shown that Ne has a spin induced by the kinetic exchange interaction. This can be regarded as one of multi-configuration effect. The v-dependence of λ can be interpreted by an induced spin on Ne, which generates from the kinetic exchange interaction. The induced spin becomes smaller as the interatomic distance increases because the integral in Eq. (IV.7), which means the overlap between 6s and 8s orbital, decreases. Since most of the observed spin-spin interaction is ascribed to the interaction between the induced spin of Ne and Rydberg electron, the spin-spin constant decrease as the induced spin decreases. As the interactomic distance decrease, the distance between a Ne and a Rydberg electron decrease and the spin-spin interaction should be increases. The observed v-dependence indicates that this increase is smaller than the decrease of induced spin on Ne. The reason is that by the exchange repulsion between Ne and Rydberg electron, the distance becomes also large as the interatomic distance increase.

IV.3. Predissociation of $^3\Sigma^+$ Hg($^3S_1$)Rg states

The predissociation are observed in $^3\Sigma^+$ Hg(9^3S_1)Ne and $^3\Sigma^+$ Hg(8^3S_1)Ar, and the lifetimes estimated line broadening are listed in Table 3. The lifetime of Hg(9^3S_1)Ne is shorter than that of Hg(8^3S_1)Ne, and the lifetime of HgNe is longer than that of HgAr at the same principal quantum

number. By the analysis of products from $^3\Sigma^+$ Hg(8^3S_1)Ar, the $^3\Sigma^+$ Hg(n^3S_1)Rg predissociates to Hg($^3D_1$ or $^3D_3$) and Rg though the Hg((n−2)^{3}D)Ne[13]. Therefore the n− and Rg−dependence of lifetime is ascribed to the overlap between the $^3\Sigma^+$ Hg(n^3S_1)Rg and the $^3\Sigma^+$ Hg((n−2)^{3}D)Ne.

V. CONCLUSION

We observed high resolution OODR spectra of 6sns electronic configuration states i.e. $^3\Sigma^+$ Hg(7^3S_1)Ne (v=0,1), $^3\Sigma^+$ Hg(8^3S_1)Ne (v=0−3) and $^3\Sigma^+$ Hg(9^3S_1)Ne (v=1−3) having a different principal quantum number (n) and a vibrational quantum number (v) each other. Their rotational transitions are assigned by simulation taking into account the Hönl−London factor of $^3\Sigma^+ - {}^3\Pi_{0^+} - {}^1\Sigma^+$ transition and laser line width. Rotational constants and spin−spin constant are determined by non−linear least square fit. We found that the spin−spin constant depends on both n and v. Although the n−dependence can be explain in terms of the distance between the Rydberg electron (ns) and the ion core electron (6s), absolute values of spin−spin constant more than ten times as large as calculation values derived form ns6s configuration. The v−dependence can not be explained by 6sns configuration, ether. Both deviation from view of a single configuration, 6sns, is ascribed to an induced spin on the closed shell Ne, and these mechanism to be induced spin is the kinetic exchange interaction. High resolution OODR spectra of $^3\Sigma^+$ Hg(8^3S_1)Ar (v = 2,14) are also observed but their rotational lines are too broad to analyze due to predissociation. The rotational lines of $^3\Sigma^+$ Hg(9^3S_1)Ne (v = 1,2,3) are broaden, too. The lifetime of $^3\Sigma^+$ Hg(9^3S_1)Ne (v=1,2,3) estimated from the line width are 40, 20, 10 ps, respectively and that of $^3\Sigma^+$ Hg(8^3S_1)Ar is < 20 ps.

ACKNOWLEDGMENTS

The present study is supported in part by a grant–in–aid from the Ministry of Education (No. 05453016).

APPENDIX

The OODR Hönl–London factor for $^3\Sigma^+$ (J) – $^3\Pi_{0^+}$ (J') – $^1\Sigma^+$ (J") can be represented by following equation

$$I \propto \sum_M \left| \left\langle {}^3\Sigma^+; F_j \middle| \mu \middle| {}^3\Pi_{0^+} \right\rangle \right|^2 \left| \left\langle {}^3\Pi_{0^+} \middle| \mu \middle| {}^1\Sigma^+ \right\rangle \right|^2 \qquad \text{(A1)}$$

where $^3\Sigma^+$ wavefunctions are expressed using basis wavefunctions $|\Lambda,S,\Sigma;\Omega,J,M\rangle$ as:

$$|{}^3\Sigma^+; F_3\rangle = -2^{-1/2} C_J[\,|0^+,1,1;1,J,M\rangle + |0^+,1,-1;-1,J,M\rangle] + S_J\,|0+,1,0;0,J,M\rangle \qquad \text{(A2)}$$

$$|{}^3\Sigma^+; F_2\rangle = 2^{-1/2} C_J[\,|0^+,1,1;1,J,M\rangle - |0^+,1,-1;-1,J,M\rangle] \qquad \text{(A3)}$$

$$|{}^3\Sigma^+; F_1\rangle = 2^{-1/2} S_J[\,|0^+,1,1;1,J,M\rangle + |0^+,1,-1;-1,J,M\rangle] + C_J\,|0+,1,0;0,J,M\rangle, \qquad \text{(A4)}$$

where

$$C_J = \left[\frac{F_2(J) - F_1(J)}{F_3(J) - F_1(J)} \right]^{1/2} \qquad \text{(A5)}$$

$$S_J = \left[\frac{F_3(J) - F_2(J)}{F_3(J) - F_1(J)}\right]^{1/2} \qquad \text{(A6)}$$

and $F_1(J)$, $F_2(J)$, $F_3(J)$ are the eigenvalues of F_1, F_2, F_3 state respectively. The $^3\Pi_{0^+}$ and $^1\Sigma^+$ wavefunctions are represented as[14]

$$|^3\Pi_{0^+}> = 2^{-1/2}\,[\,|1,1,-1;0,J',M'> + |-1,1,1;0,J',M'>] \qquad \text{(A7)}$$

and

$$|^1\Sigma^+> = |0+,0,0;0,J'',M''>. \qquad \text{(A8)}$$

The Hönl–London factors of the OODR process are derived as follows:

$$I(^RQ,P)_{J''} \propto \mu_1^2\mu_2^2 C_J^2 (J''+1) \qquad \text{(A9)}$$

$$I(^RR,P)_{J''} \propto \mu_1^2\mu_2^2 \frac{(J''+1)(4J''^2+1)}{(2J''+1)(2J''-1)} \qquad \text{(A10)}$$

$$I(^PP,P)_{J''} \propto \mu_1^2\mu_2^2 \frac{2(J''-2)(J''-1)(4J''^2+J''+12)}{(2J''+1)(2J''-1)^2} \qquad \text{(A11)}$$

$$I(^PQ,P)_{J''} \propto \mu_1^2\mu_2^2 S_J^2 (J''+1) \qquad \text{(A12)}$$

where, for example, $I(^RQ,P)J''$ is the Hönl–London factor for the successive

excitation of a P–branch ^{R}Q–branch from a ground state having a rotational quantum number (J"), μ_1 and μ_2 are factors of first and second excitation respectively, which are common for all the rotational transitions.

References

1. K.Yamanouchi, S.Isogai, M.Okunshi, and S.Tsuchiya, *J.Chem.Phys.*, **88**, 205 (1988).

2. M.Okunishi, K.Yamanouchi, K.Onda, and S.Tsuchiya, *J.Chem.Phys.*, **95**, 2675 (1993).

3. K.Onda, K.Yamanouchi, M.Okunishi, and S.Tsuchiya, to be published

4. M.C–Duval, O.B.D'Azy, W.H.Breckenridge, C.Jouvet, and B.Soep, J.Chem.Phys., 85, 6324 (1986).

5. J.K.G.Watson, *Can.J.Phys.*, **46**, 1637,(1968).

6. K.Kayama, and J.C.Baird, *J.Chem.Phys.*, **43**, 1082 (1965).

7. M.Tinkham and M.W.P.Strandberg, *Phys.Rev.*, **97**, 937 (1955).

8. K.Kayama, *J.Chem.Phys.*, **42**, 622 (1965)

9. G.Simons, *J.Chem.Phys.*, **60**, 645 (1974), I.Martin and G.Simons, *J.Chem.Phys.*, **62**, 4799 (1975).

10. E.U.Condon and G.H.Shortley, *The Theory of Atomic Spectra*, Cambridge University Press, Cambridge, 1951.

11. P.W.Anderson, *Phys.Rev.*, **79**, 350 (1950); P.W.Anderson, *Solid State Physics*, F.Seitz and D.Turnbull ed., Vol.14 (1963)

12. A.S.–C.Cheung, K.Yoshino, W.H.Parkinson, and D.E.Freeman, *J.Mol.Spec.*, **119**, 1 (1986).

13. K.Onda, C.Jouvet, S.Onoue and K.Yamanouchi, to be published.

14. J.Hougen, *NBS Monograph 115*, Nat.Bur.Stand.(US), 1970.

Table I. Rotational constants (B_v), equilibrium interatomic distance(r_e) and spin–spin constants (λ) for $^3\Sigma^+$ Hg(n^3S_1)Ne (n=7,8,9).

		B_v / cm^{-1}	r_v / Å	λ / cm^{-1}
$^3\Sigma^+$ Hg(7^3S_1)Ne	v=0	0.0980(17)	3.06(3)	0.38(5)
	v=1	0.0902(23)	3.19(4)	0.38(6)
$^3\Sigma^+$ Hg(8^3S_1)Ne	v=0	0.0983(20)	3.06(3)	0.28(5)
	v=1	0.0909(20)	3.18(3)	0.22(5)
	v=2	0.0828(23)	3.33(4)	0.20(7)
	v=3	0.0733(14)	3.54(3)	0.15(4)
$^3\Sigma^+$ Hg(9^3S_1)Ne	v=1	0.0926(53)	3.15(9)	0.00(12)

Parenthesis means a uncertainty σ derived from the non–linear least square fit.

Table II. Bandorigins for $^3\Sigma^+$ Hg(n^3S_1)Ne (n=7–9) measured from A(v=0).

		Bandorigin / cm^{-1}
$^3\Sigma^+$ Hg(7^3S_1)Ne	v=0	23087.99(5)
	v=1	23130.86(7)
$^3\Sigma^+$ Hg(8^3S_1)Ne	v=0	34436.01(5)
	v=1	34481.01(5)
	v=2	34517.50(6)
	v=3	34544.63(4)
$^3\Sigma^+$ Hg(9^3S_1)Ne	v=1	38663.85(14)

Parenthesis means a uncertainty σ derived from the non–linear least square fit.

Table III. Lifetimes for $^3\Sigma^+$ Hg(n^3S_1)Ne (n=8,9) and $^3\Sigma^+$ Hg(8^3S_1)Ar

		lifetimes / ps
$^3\Sigma^+$ Hg(8^3S_1)Ne	v=0–3	>500
$^3\Sigma^+$ Hg(9^3S_1)Ne	v=1	40
	v=2	<20
	v=3	<10
$^3\Sigma^+$ Hg(8^3S_1)Ar	v=2	<20

Table IV. Calculated and observed spin–spin constants for v=1 of $^3\Sigma^+$ Hg(n^3S_1)Ne (n=7–9)

	spin–spin constant / cm^{-1}	
	obs.	calc.
n=7	0.38(4)	0.023
n=8	0.22(3)	0.0051
n=9	0.00(12)	0.0018

Figure Captions

Fig. 1 Observed and calculated spectrum A–X (0,0) for HgNe. The broken line in the calculated spectrum is ^{202}HgNe rotational structure drawn by the analysis of reference 4. The solid line in the calculated spectrum is the second laser shape using Lorentzian function (FWHM = 0.08cm^{-1}) in order to calculate the OODR spectrum.

Fig. 2 High resolution OODR spectra and calculated rotational structure for $^3\Sigma^+$ Hg(8^{3}S$_1$)Ne (a) v=0, (b) v=1, (c) v=2 and (d) v=3) – A (v=0). The rotational constants and spin–spin constants are listed in Table 2. The rotational temperature is 2.0 K and FWHM of laser is 0.08 cm^{-1}.

Fig. 3 (a) Observed and calculated rotational structure for $^3\Sigma^+$ Hg(9^{3}S$_1$)Ne (v=1) – A (v=0). The FWHM for the calculated spectrum, 0.22 cm^{-1}, is larger than the laser line width, 0.08 cm^{-1}, due to predissociation. (b) and (c) Observed rotational structure for $^3\Sigma^+$ Hg(9^{3}S$_1$)Ne ((b) v=2, (c) v=3) – A (v=0). Both spectra are broaden by predissociation.

Fig. 4 High resolution OODR spectra and calculated rotational structure for $^3\Sigma^+$ Hg(7^{3}S$_1$)Ne (a) v=0, (b) v=1) – A (v=0). The rotational constants and spin–spin constants are listed in Table 2. The rotational temperature is 2.0 K and FWHM is 0.08 cm^{-1}.

Fig. 5 Observed rotational structure for $^3\Sigma^+$ Hg(8^{3}S$_1$)Ar (v=2) – A (v=4).

Fig. 6 The spin–spin constants, λ, for v=1 states of $^3\Sigma^+$ Hg(n^{3}S$_1$)Ne

(n=7,8,9) are plotted as a function of the mean radius of Rydberg electron, <r>.

Fig. 7 The spin–spin constants, λ, for $^3\Sigma^+$ Hg(8^3S_1)Ne (v=0–3) are plotted as a function of the interatomic distance.

Fig.1

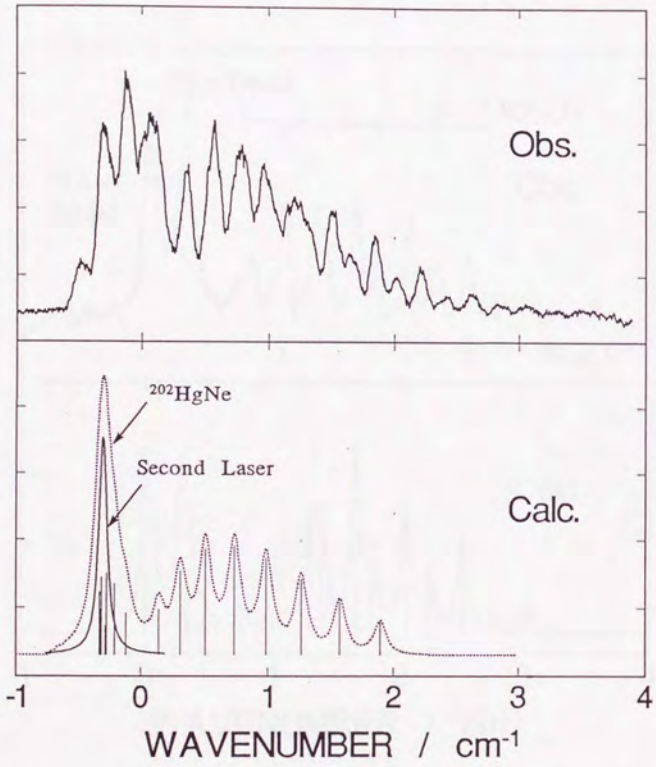

Fig.2(a)

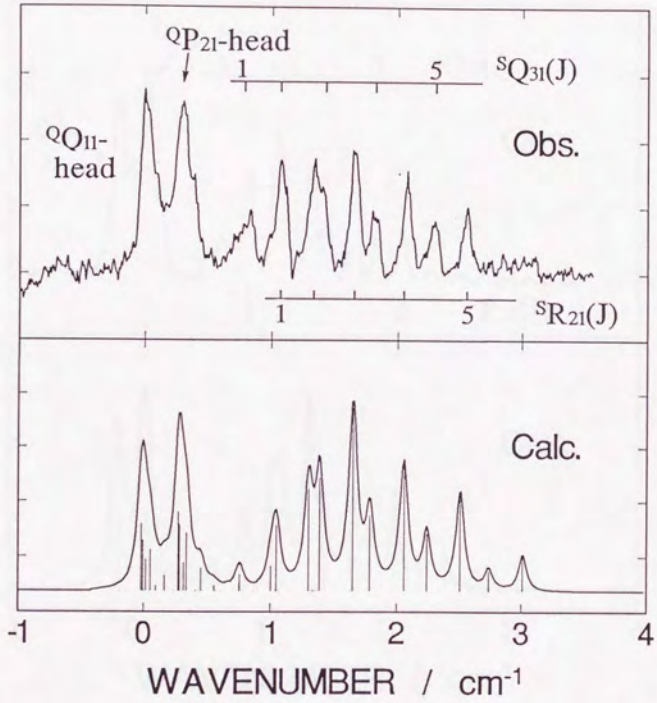
$^{Q}P_{21}$-head
1
5
$^{S}Q_{31}(J)$
$^{Q}Q_{11}$-
head
Obs.
1
5
$^{S}R_{21}(J)$
Calc.
-1
0
1
2
3
4
WAVENUMBER / cm^{-1}

Fig.2(b)

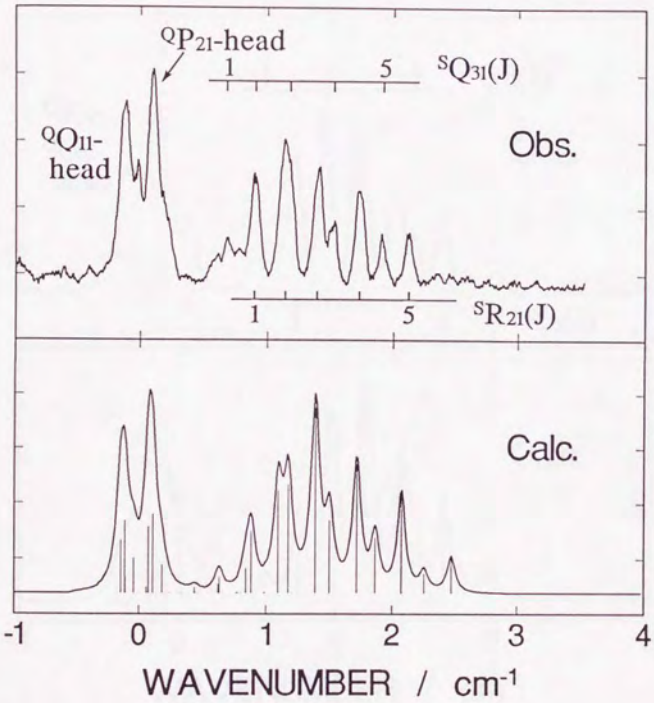
$^{Q}P_{21}$-head
1
5
$^{S}Q_{31}(J)$
$^{Q}Q_{11}$-
head
Obs.
1
5
$^{S}R_{21}(J)$
Calc.
-1
0
1
2
3
4
WAVENUMBER / cm^{-1}

Fig.2(c)

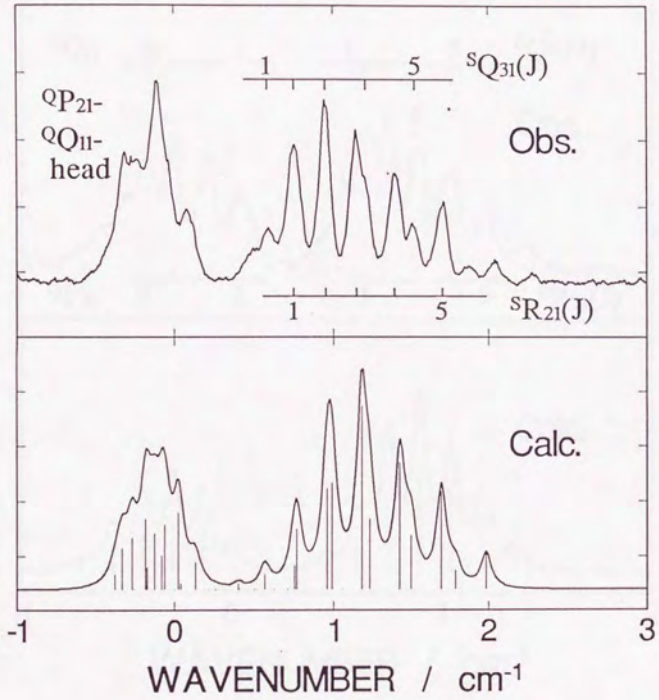
1
5
SQ31(J)
QP21-
QQ11-
head
Obs.
1
5
SR21(J)
Calc.
-1
0
1
2
3
WAVENUMBER / cm-1

Fig.2(d)

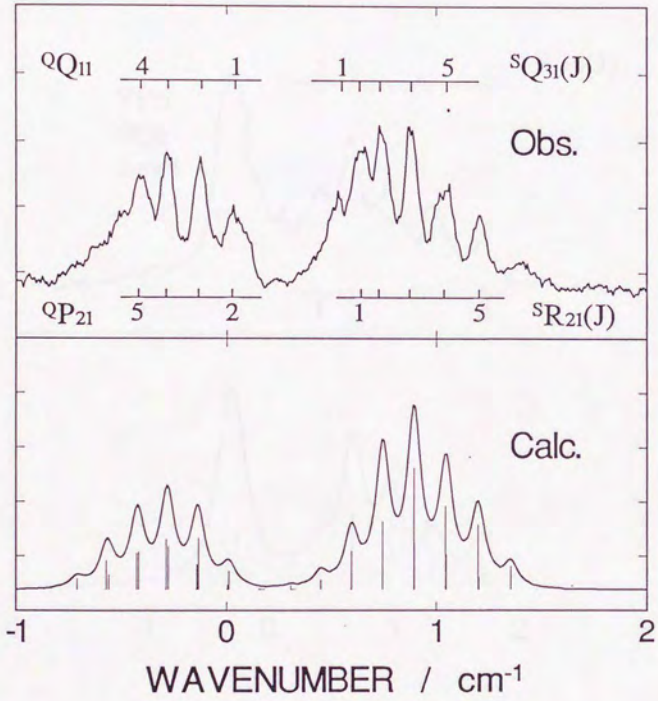
$^{Q}Q_{11}$
4
1
1
5
$^{S}Q_{31}(J)$
Obs.
$^{Q}P_{21}$
5
2
1
5
$^{S}R_{21}(J)$
Calc.
-1
0
1
2
WAVENUMBER / cm^{-1}

Fig.3(a)

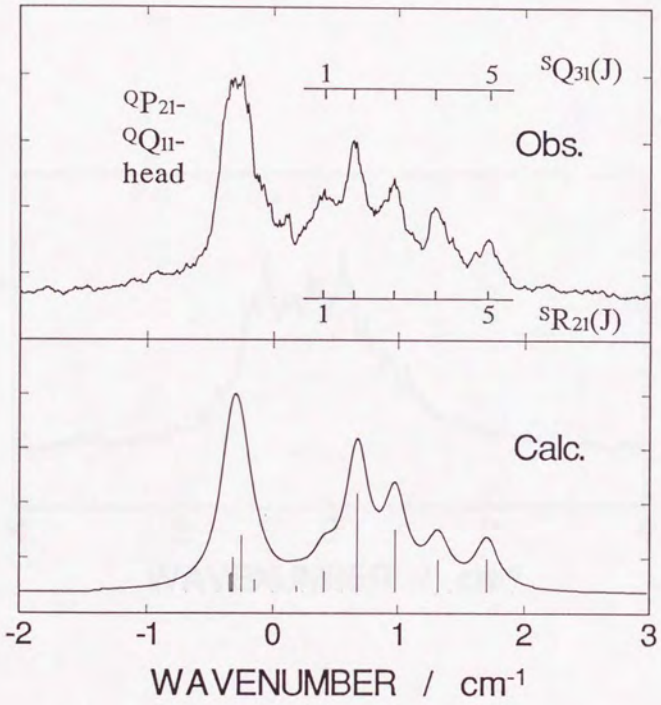
1
5
SQ31(J)
QP21-
QQ11-
head
Obs.
1
5
SR21(J)
Calc.
-2
-1
0
1
2
3
WAVENUMBER / cm-1

Fig.3(b)

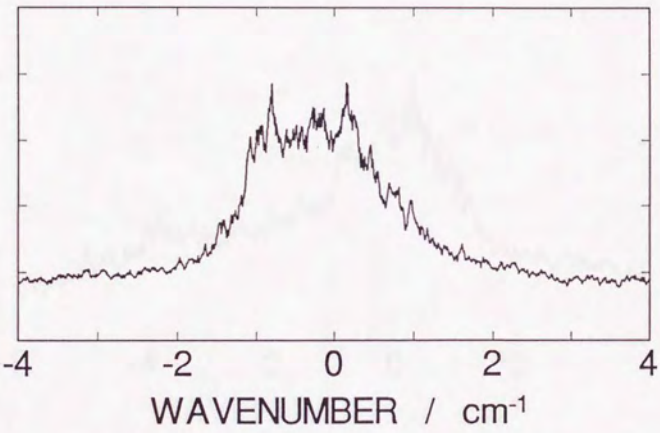

Fig.3(c)

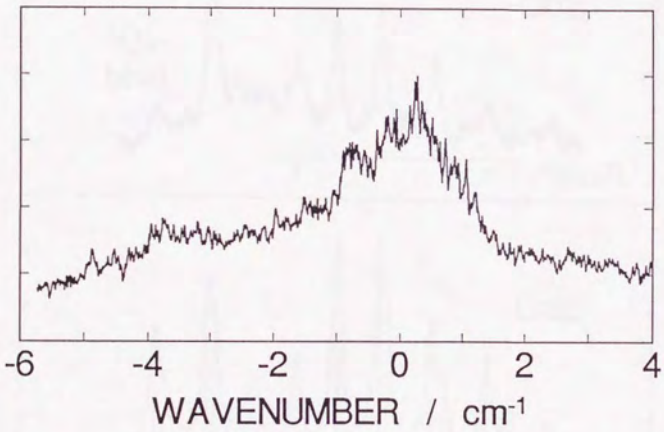

Fig.4(a)

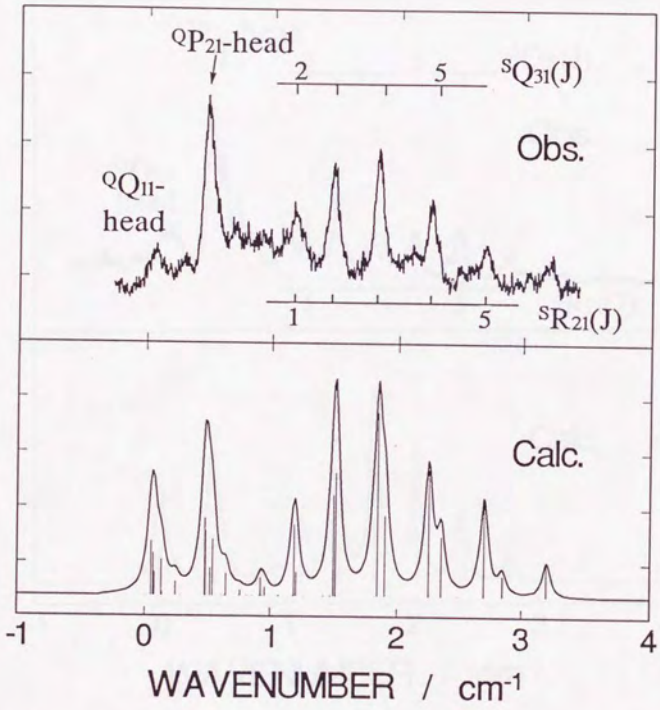
$^{Q}P_{21}$-head
2
5
$^{S}Q_{31}(J)$
Obs.
$^{Q}Q_{11}$-
head
1
5
$^{S}R_{21}(J)$
Calc.
-1
0
1
2
3
4
WAVENUMBER / cm^{-1}

Fig.4(b)

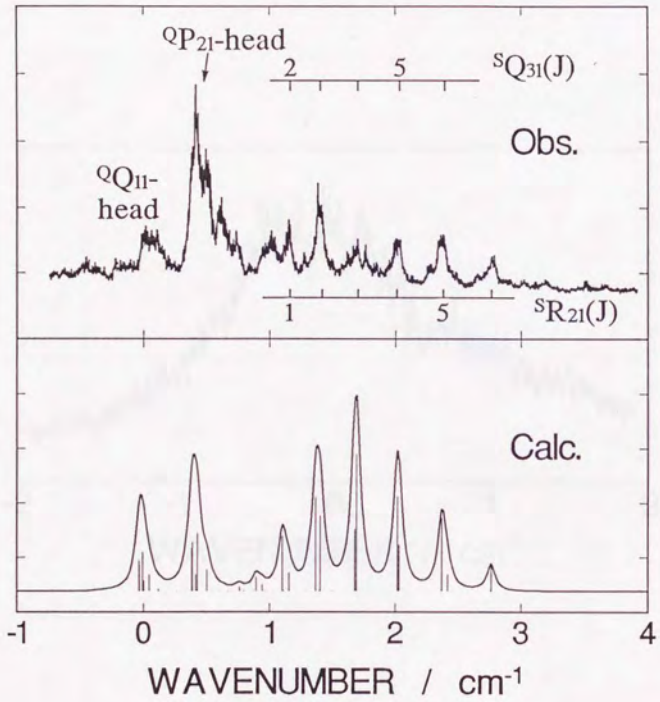
$^{Q}P_{21}$-head
2
5
$^{S}Q_{31}$(J)
Obs.
$^{Q}Q_{11}$-
head
1
5
$^{S}R_{21}$(J)
Calc.
-1
0
1
2
3
4
WAVENUMBER / cm^{-1}

Fig.5

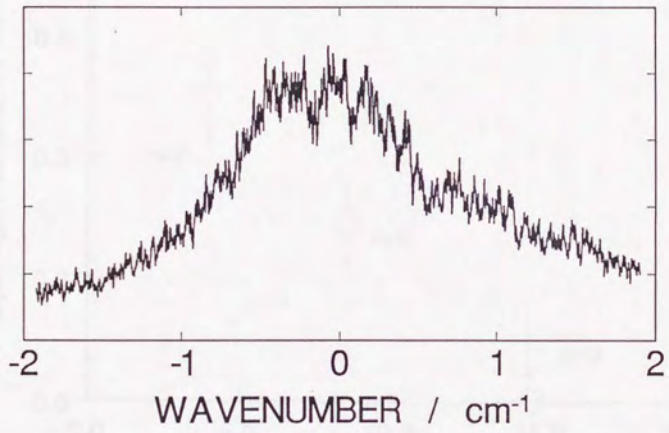

Fig.6

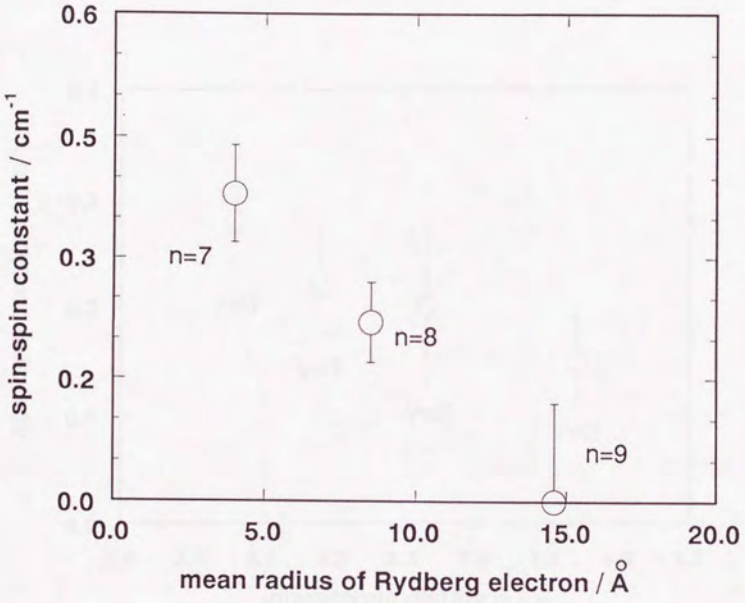
0.6
0.5
0.3
0.2
0.0
spin-spin constant / cm-1
n=7
n=8
n=9
0.0
5.0
10.0
15.0
20.0
mean radius of Rydberg electron / Å

Fig.7

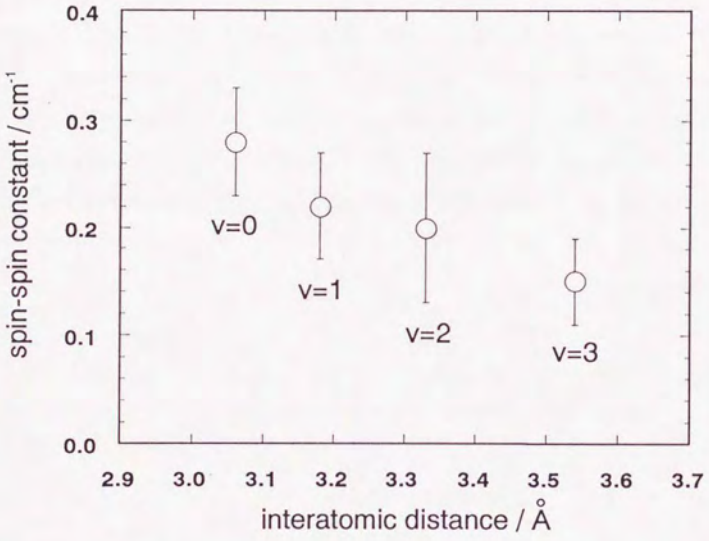
0.4
0.3
0.2
0.1
0.0
spin-spin constant / cm-1
v=0
v=1
v=2
v=3
2.9
3.0
3.1
3.2
3.3
3.4
3.5
3.6
3.7
interatomic distance / Å

Chapter 4

Interatomic potentials of Rydberg $^1\Sigma^+$ states of Hg(n^1S_0)Ne (n=7–9) van der Waals dimer

ABSTRACT

OODR spectra of $^1\Sigma^+$ Hg(n^1S_0)Ne (n=7–9) are measured via A and B states. By analysis of vibrational structure of these spectra, interatomic potentials are determined. The potential for n=7 has three quasi–bound states above the dissociation limit. The dissociation energy (D_e) defined by energy difference between a bottom of the potential and a dissociation limit is 29 cm^{-1}. For n=8, the potential (D_e=239cm^{-1}) becomes much deeper. For n=9, the potential shape is similar to that for n=8 but the D_e=297 cm^{-1} is larger. This n–dependence of the potential shape can be explained by the n–dependence of the exchange repulsion between a Rydberg electron and a rare gas in the same manner as Hg(n^3S_1)Ne Rydberg series which has the same electronic configuration, 6sns. However, the potential of singlet series is more stable than that of triplet series. It is shown that this difference is ascribed to the induced spin on Ne by the kinetic exchange interaction.

I. INTRODUCTION

Rydberg states of HgNe van der Walls dimer has investigated in order to reveal the interaction between a Rydberg electron and an ion core. Interatomic potentials of $^3\Sigma^+$ Hg(n^3S_1)Ne (n=7–10) are determined from optical–optical double resonance spectra[1,2]. From the principal quantum number dependence (n) of the potential, it is shown that the interatomic potential is characterized by the exchange repulsion between Rydberg electron and Ne. Since the exchange repulsion between Rydberg electron and closed shell Ne correlates to a density of Rydberg electron, the n–dependence of the interatomic potential can be predicted semi–quantitatively by a density of Hg Rydberg electron calculated from the quantum defect orbital.

Another interaction between a Rydberg electron and an ion core is the spin–spin interaction. The spin–spin constant (λ) are determined from the analysis of rotational structure for $^3\Sigma^+$ Hg(n^3S_1)Ne (n=7–9)[3], and the observed λ is too large for Rydberg state. This large spin–spin interaction between Rydberg electron and ion core electron is ascribed that the most of the spin–spin interaction generates form the interaction with induced spin on Ne. The vibrational quantum number (v) dependence of λ also indicates the existence of the induced spin on Ne. Since the induced spin on Ne depends on the interatomic distance, the spin–spin interaction between the Rydberg electron and the induced spin depends on v.

In this study, in order to get more information on the induced spin on Ne, the singlet Rydberg series are observed, and singlet and triplet potential are compared. The interatomic potential is characterized by exchange repulsion between Rydberg electron and electrons of Ne, so the direction of spin on Ne

should be reflected on the interatomic potential. The $^1\Sigma^+$ Hg(n^1S_0)Ne (n=7–9) are observed by the optical–optical double resonance method From the analysis of vibrational structure, the interatomic potentials are determined. Compared with the potential of $^3\Sigma^+$ Hg(n^3S_1)Ne (n=7–9), it is shown that the induced spin exits on Ne.

II. Experiment

The optical–optical double resonance (OODR) spectra are measured by the almost the similar set up to the triplet series was observed[1–3]. The HgNe is produced in a supersonic expansion of Ne carrier gas through a heated pulse valve with Hg reservoir. The temperature of the pulse valve and Hg reservoir is ~200℃ and the stagnation pressure is ~7 atom. The HgNe is excited to Rydberg state by OODR process using frequency–double output of two dye lasers (Lambda Phisik FL3002 and Molectron DL14P). Both dye laser are pumped by XeCl excimer laser (Lambda Physik LPX 105i) simultaneously. The fluorescence from the Rydberg states is detected by a photomultiplier (Hamamatsu R928) with a filter (Toshiba UV35) which cut the fluorescence from the intermediate states. The resolution of the doubled dye laser is ~0.8 cm–1, and the wavelength is calibrated by atomic transition of Hg.

III. Results

III.1. Interatomic potential of $^1\Sigma^+$ Hg(7^1S_0)Ne

Intermediate states for OODR process are A and B states correlated to the Hg(6^3P_1). The potential of A state has a shorter equilibrium interatomic distance (r_e) than that of B state, r_e are 3.45 and 4.92Å, respectively[4]. By

using these two state having different r_e each other, a wide interatomic region of Rydberg potential can be observed. From v=0,1 of A state, Rydberg potential in the interatomic distance of 3 – 4.5 Å is observed, and from v=0 and 1 of B state, its interatomic distance is 4 – 7.5 Å.

The observed OODR spectra via A (v'=0,1) and B (v'=0) are shown in Fig.1 (a)–(c). In this paper, the v, v', and v" stand for the vibrational quantum number of Rydberg, intermediate, and ground state, respectively. The vibrational structure in the spectrum via A (v'=0) (Fig.1 (a)) consists of four peaks and the spacing between peaks are 53.6, 45.2, and 34.3 cm^{-1}. The intensity pattern has no node because the wavefunction of v'=0 is reflected. The spectrum via A (v=1) (Fig.1 (b)) has five peaks and one node reflecting the wavefunction of v=1. The peak in the highest energy is broad because of bound free type transition. The spacing of spectrum via v=1 without the broad peak are 53.7, 45.0, and 34.2 cm^{-1}, so vibrational quantum numbers (v) of four peaks via A(v'=0) are identical to v of the four peaks via A(v'=1). Since the both progression starts suddenly, the lowest energy peak is assigned to v=0. On the other hand, the transition from B (v"=0) state is very weak but bound free type transition is observed (Fig.1 (c)). This bound free transition shows that the potential has repulsive wall in longer interatomic distance, > 4Å, that is the potential lies above the dissociation limit. Position of dissociation limit can be estimated from sum of Hg 7^1S_0–6^1S_0 transition energy and D_0 of HgNe ground state. The dissociation limit shows in Fig.1 as an arrow. Since the arrow in spectra via A (v'=0,1) is located between v=0,1 and the arrow in spectrum via B(v'=0) is located at lower energy of the broad peak, the most of potential lies above its dissociation limit.

The Birge–Sponer (BS) plot is drawn in Fig.2(a). The spacing

decreases linearly, so the potential is determined based on Franck–Condon (FC) calculation using Morse function. By using ω_e and $\omega_e x_e$ determined from the BS plot, FC factor is calculated as a parameter of r_e and r_e is estimated by trial–and–error method. The FC factor optimized and the determined parameters for Morse function are ω_e = 63.8 (1) cm−1, $\omega_e x_e$ = 4.88(55) cm^{-1}, and r_e = 2.92 (3) Å. The potential of $^1\Sigma^+$ Hg(7^1S_0)Ne is shown in Fig.4, and the potential parameters are listed in Table I.

III.2. Interatomic potential of $^1\Sigma^+$ Hg(8^1S_0)Ne

OODR spectra of $^1\Sigma^+$ Hg(7^1S_0)Ne via A (v'=0,1,2) and B (v'=0,1,2) are observed and the spectra via A (v'=0,1) and B (v'=1) are shown in Fig.4 (a)–(c). There are four peaks in the spectrum via A (v'=0) and the spacing decrease gradually, and intensity pattern reflects a wavefunction of A (v'=0). The spectrum via A(v'=1) has four peaks and the spacing between the second and third from the lowest peak in energy is much larger than the others. This large spacing reflects a node of a wavefunction of A (v'=1), i.e. one peak misses in the large spacing because of the no Franck–Condon overlap. The spacing between the lowest two peaks in the spectrum via A (v'=0) and A (v'=1) are 49.8 and 49.7 cm^{-1}, respectively. The spacing between the second and the third from the lowest peak in energy in spectrum via A(v'=0) and A(v=1) are 76.1 and 76.0 cm^{-1}. Therefore, the four peaks from the lowest peak in energy in the spectrum via A(v'=1) are identical to the four peaks in the spectrum via A(v'=0). The progression via A(v'=1) starts suddenly, so we assigned the lowest peak as v=0.

As shown in Fig.4 (c), the spectrum via B(v'=1) has simple progression if the one missing peak by the node of intermediate state includes. The

spacing between lowest two peak is 25.8 cm^{-1} of this spectrum but the highest two peaks in the spectrum via A(v'=1) is 31.1 cm^{-1}, so both progression does not overlap. In order to assign the peaks in the spectra via B (v'=0,1), the energy from X (v"=0) are estimated. The energy of v=4 is 74385.5 cm^{-1} and the lowest peak in the spectrum via B(v=1) is 74386.2 cm−1, so these peaks are identical. Based on this assignment, all peaks in the spectra via B(v'=0,1) are assigned.

The potential of this state is determined by following method. First of all, in order to know the vibrational quantum number dependence of the spacing, Birge−Sponer is plotted in Fig.2(b). The spacing decreases linearly and steeply form v=0 to 5 and the spacings of more than 5 are deviated from the line drawn from the spacings less than v=5. The decrease of spacing of more than v=5 becomes gradually. The RKR method[5] can be applied to be estimated the potential width ($r_+ - r_-$) of each vibrational state from the spacings, but in order to determine the potential, it is necessary to estimate the interatomic distance of each vibrational state. So the next step is to determine the inner wall of the potential using Morse function. Assuming the potential shape is Morse function from v=0 to 5, that is the linear part of BS plot. The ω_e and $\omega_e x_e$ can be estimated from the BS plot. Using these parameter, ω_e and $\omega_e x_e$, the equilibrium distance (r_e) is estimated from trial−and−error fit of the Franck−Condon pattern. The inner wall of the Morse function is assumed to be the observed potential. And finally, the outer wall is drawn by connecting the points of r_+ whose r_- put on the Morse function's inner wall. The potential of $^1\Sigma^+$ Hg(7^1S_0)Ne is shown in Fig.4.

III.3. Interatomic potential of $^1\Sigma^+$ Hg(9^1S_0)Ne

OODR spectra of $^1\Sigma^+$ Hg(9^1S_0)Ne via A(v'=0,1,2) and B(v'=0,1,2) are observed. As shown in Fig.5(a), five vibrational states are observed in the spectrum via A(v'=0) except a peak pointed by an arrow because this peak is the v=4 state of $^3\Sigma^+$ Hg(9^3S_1)Ne. The peak just above the v=4 of triplet potential also looks like one peak of the triplet progression, and the energy is the same as v=5 of triplet state. However, this peak should be assigned to one of singlet progression because the shape of this peak is the same as the other singlet peaks. There are six vibrational states in the spectrum via A(v'=1), but two states are missed. One state berries in the v=5 peak of triplet state pointed by the right side arrow, and the other state has no Franck–Condon overlap due to a node of wavefunction of A (v'=1). The progression of the spectra via B (v'=0,1,2) are smoothly connected with the progression of the spectra via A(v'=0,1,2).

The potential is determined by the same way of $^1\Sigma^+$ Hg(8^1S_0)Ne but the assignment of v=0. As shown in BS plot (Fig.2(c)), the vibrational spacing decreases linearly from v=0 to 5 and the spacing is deviated gradually above v=5. The $\omega_e x_e$ is determined from the slop drawn from v=0 to5. The vibrational assignment and r_e are determined by trial–and–error fit of the Franck–Condon factor using Morse function. The inner wall of this Morse function is used as an innerwall of the observed potential. Potential widths, $r_+ - r_-$, are calculated by RKR method, and the outer wall is drawn by connecting the r_+ putting on the innerwall of the Morse function. The potential of $^1\Sigma^+$ Hg(8^1S_0)Ne is shown in Fig.4 and the parameters are listed in Table I.

IV. DISCUSSION

IV.1. Principal quantum number dependence of $^1\Sigma^+$ potential

As shown in Fig.4, the interatomic potential of $^1\Sigma^+$ Hg(n^1S_0)Ne (n=7–9) depends on the principal quantum number (n). The potential of n=7 is located above dissociation limit and the potential becomes deeper as n increase. This type of n–dependence is similar to the dependence of $^3\Sigma^+$ Hg(n^3S_1)Ne Rydberg series[1], so the same model is applied to $^1\Sigma^+$ Hg(n^1S_0)Ne Rydberg series. The interatomic potential of Rydberg state (V_{Ryd}) can be written by following equation.

$$V_{Ryd} = V_{ion} + R_{ex} \qquad (1)$$

where V_{ion} is the interatomic potential of $HgNe^+$, and R_{ex} is the exchange repulsion between Rydberg electron and rare gas atom. The ion core potential, V_{ion}, consists of strong bounding force and independent of the Rydberg electron. The exchange repulsion, R_{ex}, make the potential unstable and depends on the density of the Rydberg electron. Therefore, the density of electron predicts the shape of Rydberg potential. The wavefunction of Rydberg state can be calculated from quantum defect, that is the quantum defect orbital (QDO)[6,7].

Fig.6 shows the density of Hg (n^1S_0) (n=6–9) Rydberg electron calculated from the Hg's quantum defect. The interatomic distance region of the observed potential is from 3 to 7 Å, so the density of Rydberg electron in this region determine the shape of the Rydberg potential. At n=6, the most of electron density concentrates within 2.5 Å, so the ion core and the electron make neutral atom and the interatomic force between neutral Hg and Ne is

dispersion force. At n=7, the density of electron is highest from 2 – 6 Å, and the potential lies above dissociation limit by strong repulsive force. In the case of n=8, the hump of density around 8 Å and the potential has a hump there. The density becomes almost zero from 2.5–7 Å so the potential is almost the same as $HgNe^+$ potential (V_{ion}).

IV.2. Comparison between $^1\Sigma^+$ and $^3\Sigma^+$ potentials

The $^3\Sigma^+$ $Hg(n^3S_1)Ne$ consists of the same electronic configuration as $^1\Sigma^+$ $Hg(n^1S_0)Ne$, that is 6sns. If the potential can be predicted by sum of the ion core potential (V_{ion}) and the exchange repulsion between Hg's Rydberg electron and Ne (R_{ex}), both singlet and triplet should be the same. In order to compare between singlet and triplet, the dissociation energy (D_e) is plotted as a function of effective principal quantum number (n^*) in Fig.7. Although D_e are almost the same at n=8 and 9, D_e at n = 7 is are very different. The origin of difference between triplet and singlet is exchange interaction between 6s and ns, but the main interaction between ns and ion core at n=7 is the exchange repulsion with Ne from above analysis. Therefore, the difference of potentials between singlet and triplet can be explained taking into account the direction of spin on Ne atom. The state which the direction of spin on Ne is parallel to Rydberg electron and both orbitals are not orthogonal is more unstable than the state which the two spins are anti–parallel. Kinetic exchange interaction can predicts that the direction of spin on Ne is the same as 6s. The mechanism of the kinetic exchange interaction is that Ne's electron transfer to Hg^+'s 6s orbital through small overlap between 6s and 2p of Ne. The ion core consists of Hg^+ and Ne, so 6s orbital can contain one more electron whose direction should be different by Pauli's

principal. After anti-parallel electron transferred to 6s, more parallel electron remains on Ne then anti-parallel electron. Therefore, the parallel spin to 6s is induced on Ne. The energy of kinetic exchange interaction is shown by[8,9]

$$\Delta E = -\frac{2b(R)^2}{U} \quad , \qquad (2)$$

where ΔE is the energy difference between parallel and anti-parallel electrons of two atoms, b(R) is the parameter depends on overlap between two orbital i.e. 6s and 2p, and U is energy difference between two orbital. One of material having the similar U to $HgNe^+$ is NiO and NiO has a anti-ferromagnetism by kinetic exchange interaction. Assuming the overlap (b(R)) is the same between $HgNe^+$ and NiO, since the U of $HgNe^+$ is half of NiO, i.e. 12eV and 6eV, respectively[10], the energy of kinetic exchange interaction of $HgNe^+$ is estimated half of NiO. The energy of exchange interaction between two Ni^{2+} through O^{2-} by kinetic exchange interaction is 34 cm^{-1} [11], so the energy caused by kinetic exchange interaction seems to be enough to make difference between triple and singlet potentials.

V. Summary

We measured OODR spectra of $^1\Sigma^+$ $Hg(n^1S_0)Ne$ (n=7-9), and determined the interatomic potentials by analysis of vibrational structure. It is shown that the principal quantum number dependence of the interatomic potential can be explained by the density of electron calculated from the quantum defect orbital. However, the potential of n=7 is different from triplet potential having the same electronic configuration. This difference is

ascribed to the induced spin on Ne, i.e. if the induced spin is anti-parallel to the Rydberg electron, the exchange interaction between Rydberg electron and the induced spin becomes small. The mechanism to induced spin on Ne is the kinetic exchange interaction.

ACKNOWLEDGMENTS

The present study is supported in part by a grant-in-aid from the Ministry of Education (No. 05453016).

REFERENCES

1. K.Onda, K.Yamanouchi, M.Okunishi, and S.Tsuchiya, to be published.

2. M.Okunishi, K.Ymanouchi, K.Onda, and S.Tsuchiya, *J.Chem.Phys.*, **95**, 2675 (1993).

3. K.Onda and K.Yamanouchi, to be published.

4. K.Yamanouchi, S.Isogai, M.Okunishi, and S.Tsuchiya, *J.Chem.Phys.*, **88**, 205 (1988).

5. H.E.Fleming and K.N.Rao, *J.Mol.Spec.*, **44**, 189 (1972).

6. G.Simons, *J.Chem.Phys.*, **60**, 645 (1974).

7. I.Martin and G.Simons, *J.Chem.Phys.*, **62**, 4799 (1975).

8. P.W.Anderson, *Phys.Rev.*, **79**, 350 (1950).

9. P.W.Anderson, *Solid State Physics*, F.Seitz and D.Turnbull ed., Vol.14 (1963).

10. P.A.Cox, *The Electronic Structure and Chemistry of Solids*, Oxford University Press, Oxford, (1987).

11. J.Smart, *Magnetism III,* ed. by G.Rado and H.Suhl, Academic Press (1963).

Table I. Potential parameters for the $^1\Sigma^+$ Hg(n^1S_0)Ne (n=6–9).

	ω_e / cm^{-1}	$\omega_e x_e$ / cm^{-1}	D_e / cm^{-1}	r_e/Å
$^1\Sigma^+$ Hg(6^1S_0)Ne[a]	10.5	1.6	46	3.90
$^1\Sigma^+$ Hg(7^1S_0)Ne	63.9(10)[b]	4.88(20)[b]	29(2)[c]	2.93(3)[d]
$^1\Sigma^+$ Hg(8^1S_0)Ne	59.5(5)[b]	4.37(10)[b]	239(2)[c]	2.98(3)[d]
$^1\Sigma^+$ Hg(9^1S_0)Ne	57.0(3)[b]	3.18(5)[b]	297(2)[c]	2.96(3)[d]

[a]reference 4.

[b]the error is an uncertainty σ of the least square method.

[c]the error is estimated from Eq.(1).

[d]the error is estimated from trial–and–error FC simulation.

FIGURE CAPTIONS

Fig.1. Observed OODR spectra of $^1\Sigma^+$ Hg(7^1S_0)Ne. The intermediate states are (a) A(v=0), (b) A(v=1), and (c) B(v=0). The wavenumber means the energy measured from the X (v=0) state.

Fig.2. BS plot for $^1\Sigma^+$ Hg(n^1S_0)Ne (a) n=7, (b) n=8, and (c) n=9. Straight line is drawn by the least square method using v=0–4 for n=7, v=0–5 for n=8 and v=0–6 for n=9. The constants, ω_e, $\omega_e x_e$, are listed on Table I.

Fig.3. Potential curves for $^1\Sigma^+$ Hg(n^1S_0)Ne (a) n=7, (b) n=8, and (c) n=9.

Fig.4. Observed OODR spectrum of $^1\Sigma^+$ Hg(8^1S_0)Ne via (a) A(v=0), (b) A(v=1), and (c) B(v=0). The wavenumber means the energy measured from the X (v=0) state.

Fig.5. Observed OODR spectrum of $^1\Sigma^+$ Hg(9^1S_0)Ne via (a) A(v=0), (b) A(v=1), (c) B(v=0) and (d) B(v=1). The wavenumber means the energy measured from the X (v=0) state.

Fig.6. The density of electron, $|rR(r)|^2$, of Hg(6^1S_0) and Hg(n^3S_1) (n=7–10) are plotted as a function of a radius of Rydberg electron. The wavefunction, rR(r), is calculated based on Simons's quantum defect orbital[6,7].

Fig.7. Dissociation energies (D_e) of $^3\Sigma^+$ Hg(n^3S_0)Ne (n=7–10) and $^1\Sigma^+$ Hg(n^1S_0)Ne (n=7–9) are plotted as a function of n^*. n^* is defined by $n-\delta$,

where n is principal quantum number and δ is quantum defect.

Fig.1(a)

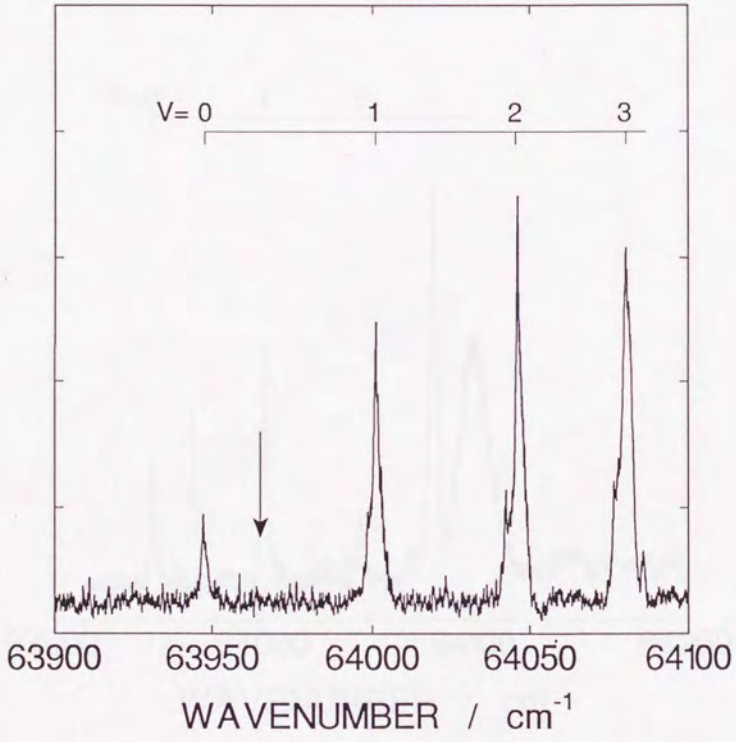

Fig.1(b)

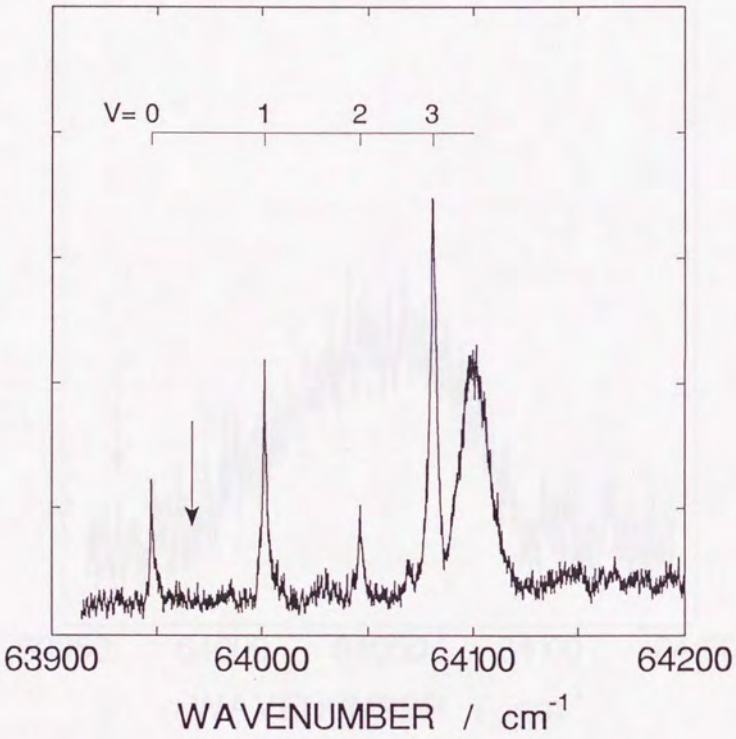

Fig.1(c)

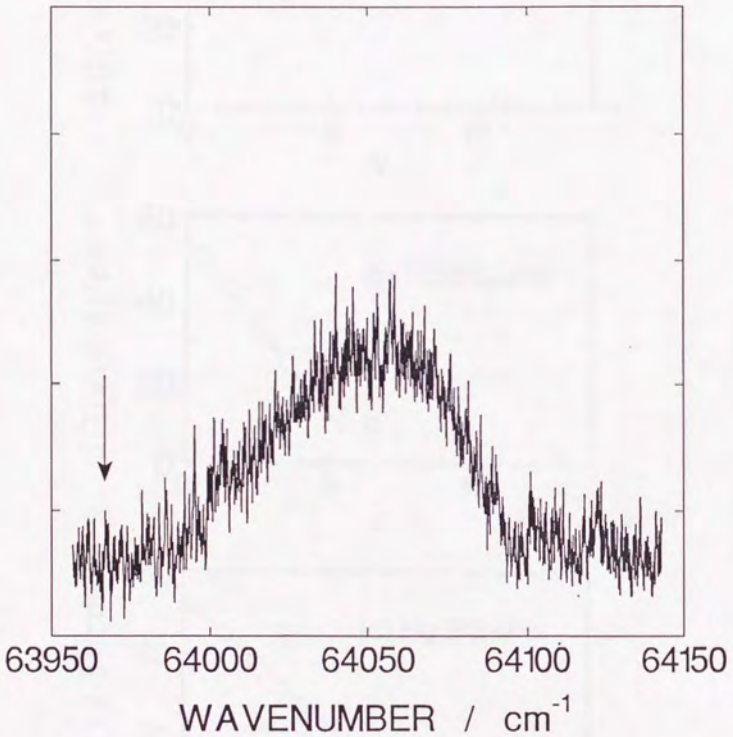

Fig.2

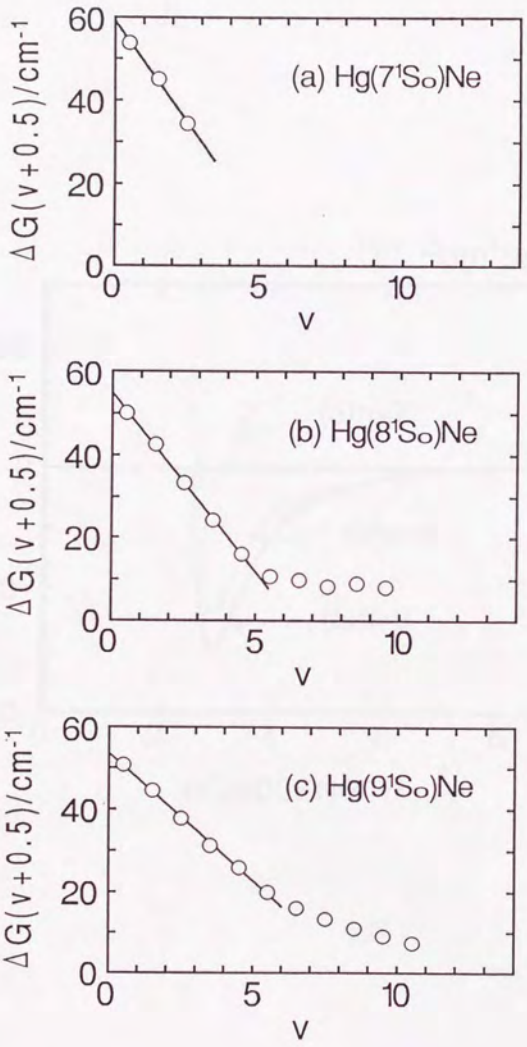

Fig.3

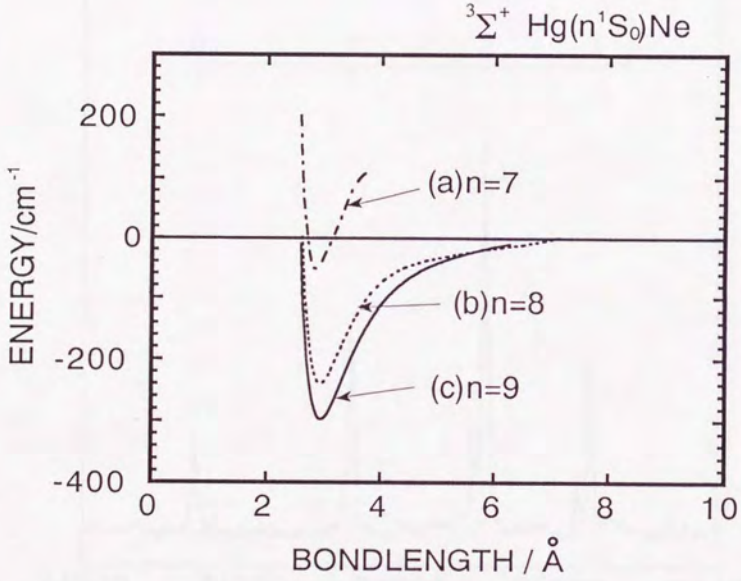
$^3\Sigma^+$ Hg(n^1S_0)Ne
200
0
-200
-400
ENERGY/cm^{-1}
(a)n=7
(b)n=8
(c)n=9
0
2
4
6
8
10
BONDLENGTH / Å

Fig.4(a)

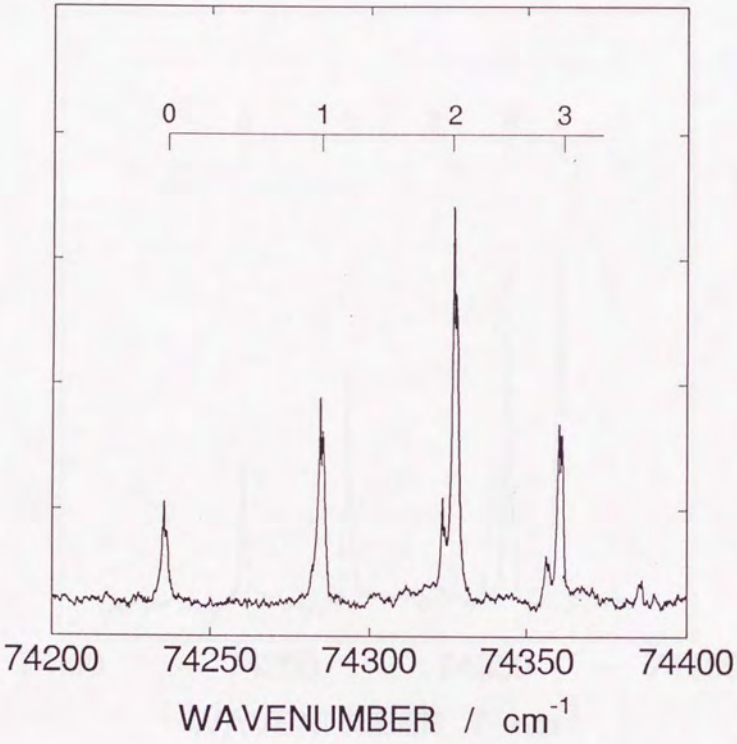

Fig.4(b)

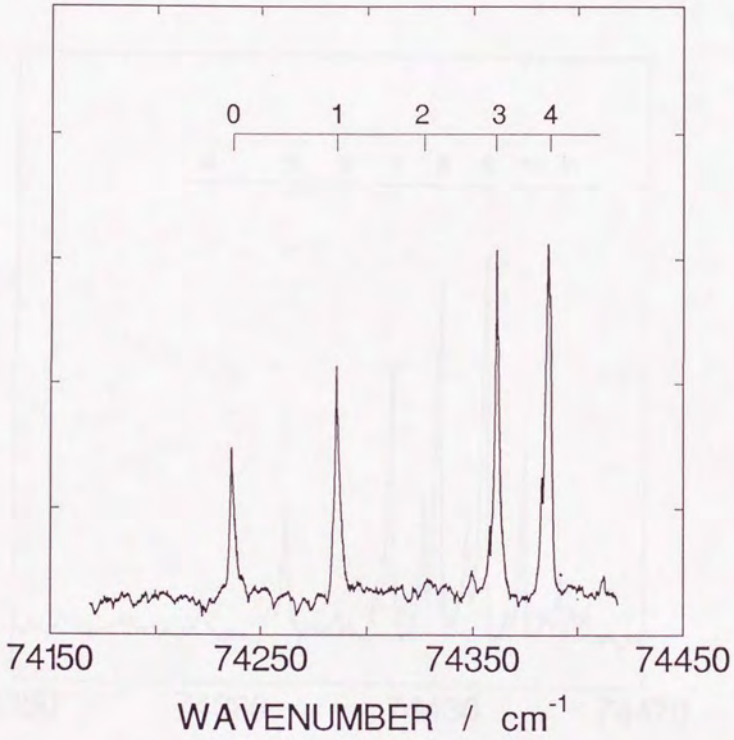

Fig.4(c)

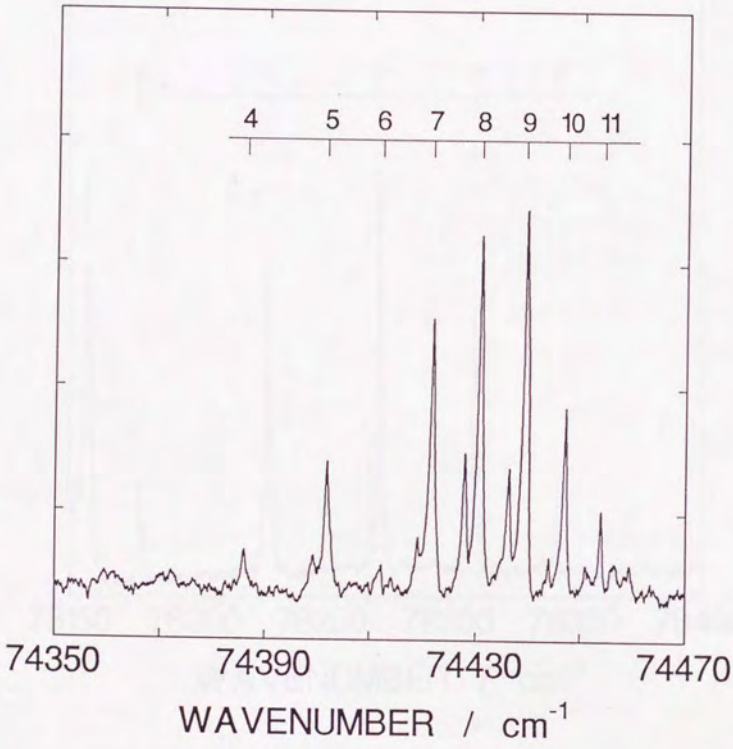

Fig.5(a)

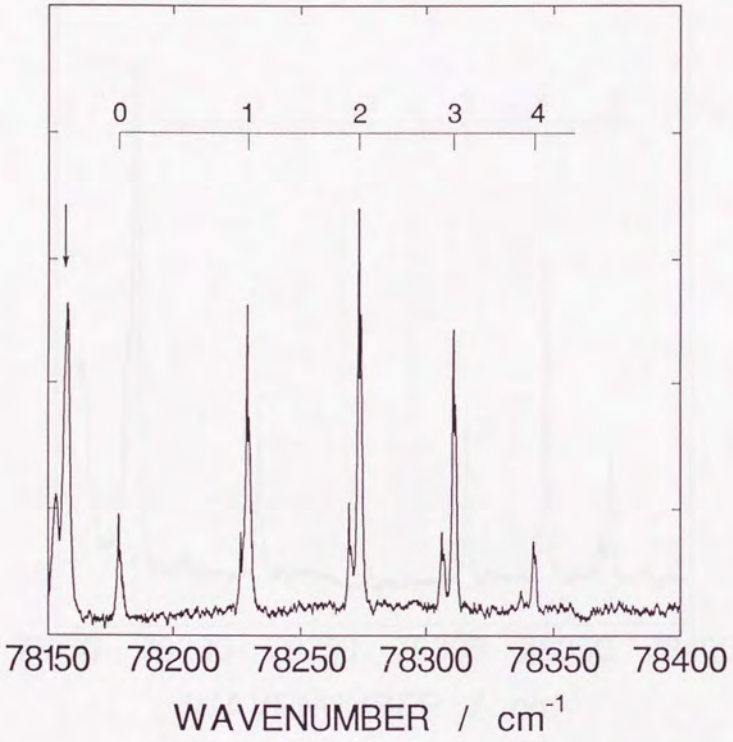

Fig.5(b)

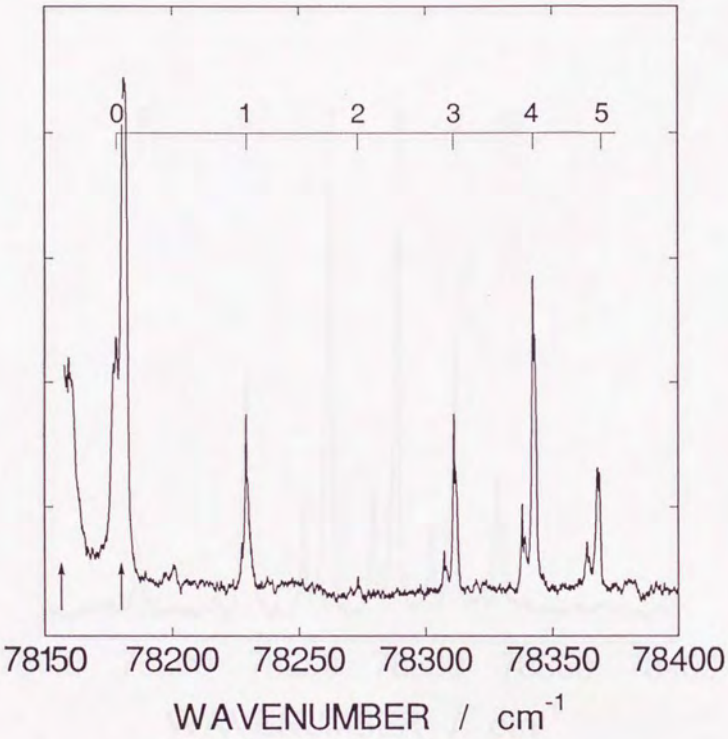

Fig.5(c)

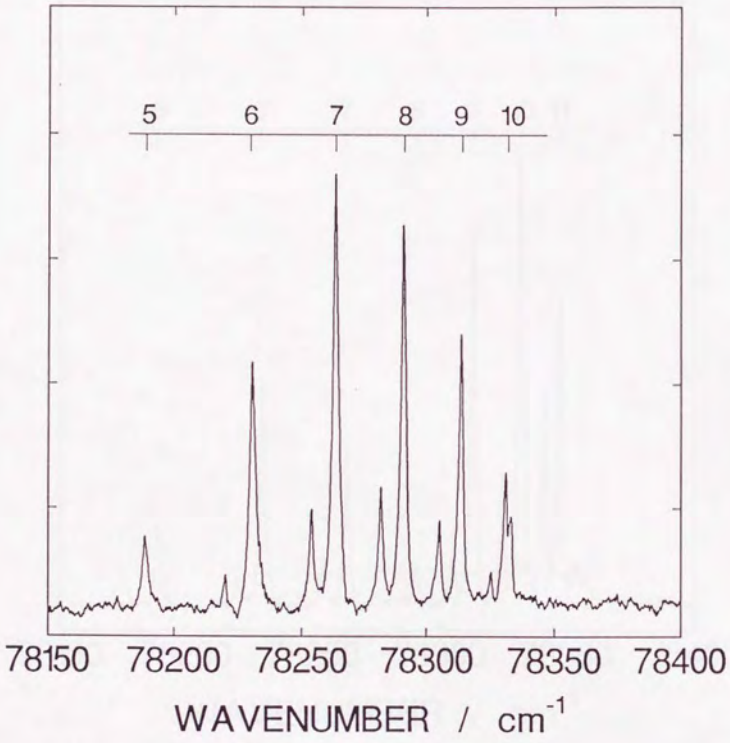
5
6
7
8
9
10
78150
78200
78250
78300
78350
78400
WAVENUMBER / cm-1

Fig.5(d)

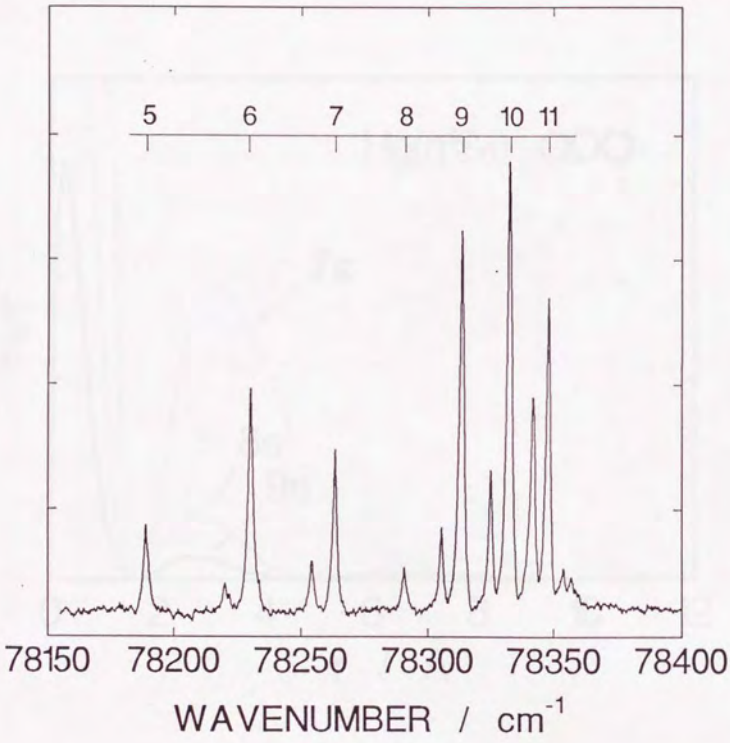
5
6
7
8
9
10
11
78150
78200
78250
78300
78350
78400
WAVENUMBER / cm-1

Fig.6

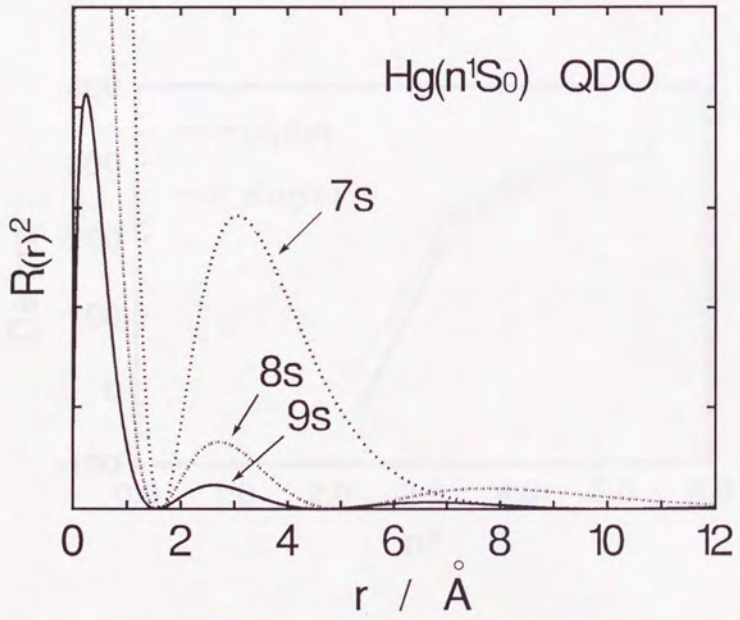

Fig.7

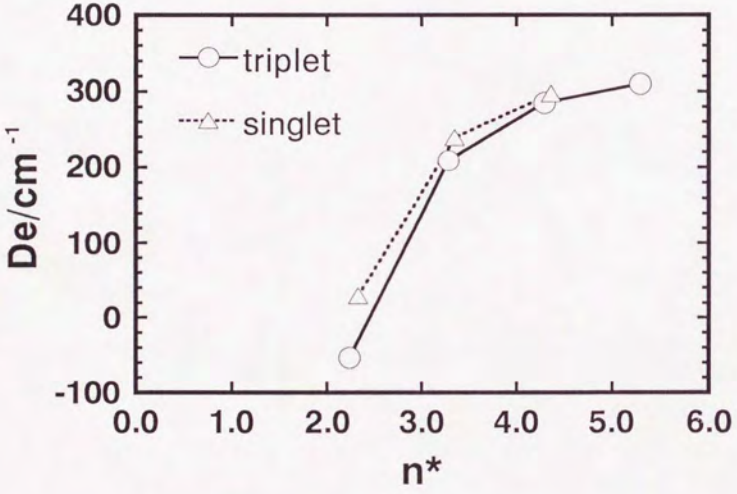
triplet
singlet
De/cm -1
400
300
200
100
0
-100
0.0
1.0
2.0
3.0
4.0
5.0
6.0
n*

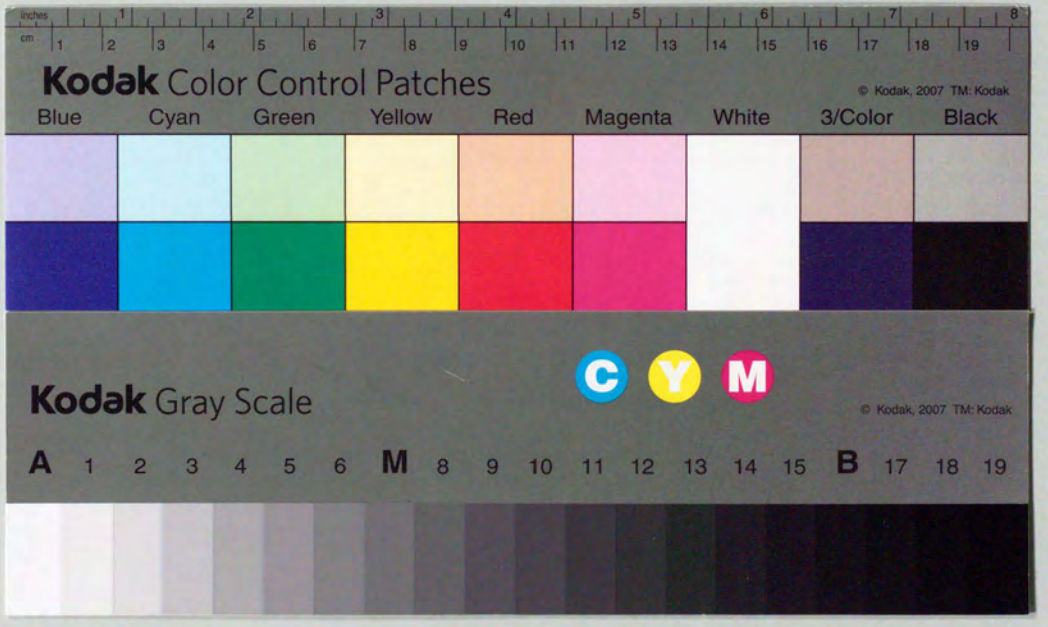
inches
cm
Kodak Color Control Patches
© Kodak, 2007 TM: Kodak
Blue
Cyan
Green
Yellow
Red
Magenta
White
3/Color
Black
Kodak Gray Scale
C
Y
M
© Kodak, 2007 TM: Kodak
A 1 2 3 4 5 6 M 8 9 10 11 12 13 14 15 B 17 18 19